Blood Distribution and Energy Metabolism of the Brain of Polar cod (*Boreogadus saida*) Under Ocean Acidification

Erasmus Mundus International M.Sc. in Marine Biological Resources (IMBRSea)
Applied Ecology and Conservation

Alfred-Wegener-Institute, Helmholtz-Centre for Polar and Marine Research
Division Biosciences
Section Integrative Ecophysiology

Thesis candidate: Jan Phillipp Geißel, B.Sc.
Reference number: 20170579
janphillipp.geissel@imbrsea.eu

Thesis supervisor: Dr. Christian Bock

presented the 05th of August 2019

Erasmus Mundus
ALFRED-WEGENER-INSTITUT HELMHOLTZ-ZENTRUM FÜR POLAR- UND MEERESFORSCHUNG
HELMHOLTZ RESEARCH FOR GRAND CHALLENGES

Declaration of authorship

I hereby declare that the thesis submitted is my own work. All direct or indirect sources used are acknowledged as references.

Data ownership

No data can be taken out of this work without prior approval of the thesis supervisor and the author.

Table of contents

I. Abbreviations and symbols III

II. Figures IV

III. Tables I

1 Executive summary 1

2 Abstract 1

3 Introduction & Aims 1

3.1 Ocean Warming and Acidification (OWA) and Ecological Consequences 1

3.2 Model species 3

3.3 Cellular energy metabolism, acid-base regulation, intracellular pH 3

3.4 Blood distribution 4

3.5 Magnetic Resonance Imaging (MRI) 6

3.6 ^{31}P-NMR Spectroscopy 7

3.7 Aims 10

4 Materials & Methods 11

4.1 Specimens and animal maintenance 11

4.2 Water supply and seawater chemistry 12

4.3 Experimental setup and protocol 13

4.4 Nuclear magnetic resonance imaging and spectroscopy 15

4.4.1 Experimental protocol 15

4.4.2 MR imaging and spectroscopy protocol 16

4.4.3 Image Analysis 17

4.4.4 Statistical analysis 20

5 Results 21

5.1 Brain morphology 21

5.2 Blood Flow and Perfusion 23

5.2.1 Vascular morphology 23

5.2.2 Angiography scans 23
5.3 *In vivo* measurement of blood distribution of the brain of polar cod 26
5.3.1 Method Application 26
5.4 *In vivo* measurement of intracellular pH and the energy metabolism of the brain of polar cod 40
5.4.1 Indices for the cellular energetic state *in vivo* 40
5.4.2 *In vivo* measurement of intracellular pH and the energy metabolism of the brain of polar cod 44
6 Discussion 48
6.1 Method Development and Evaluation 48
6.2 Effects of Ocean Acidification 50
7 Conclusion 56
8 Acknowledgements 57
9 References 58
10 Annex 64
10.1 Phantom trials 64
10.1.1 Titration curve 65

I. Abbreviations and symbols

ASL	arterial spin labelling
ATP	adenosine tri-phosphate
B_0	magnetic field, represents net magnetization vector in MRI
BOLD	blood oxygenation level dependent
CASL	continuous ASL
CBF	cerebral blood flow
CBV	cerebral blood volume
cm	centimetre
FAIR	flow-sensitive alternating inversion recovery
FLASH	fast low angle shot
FID	free induction decay
fMRI	functional MRI
IPCC	Intergovernmental Panel on Climate Change
MIP	maximum intensity projection
MR	magnetic resonance
MRI	magnetic resonance imaging
MTT	mean transit time
NMR	nuclear magnetic resonance
OA	ocean acidification
OW	ocean warming
OWA	ocean warming and acidification
PASL	pulsed ASL
pCO_2	partial pressure carbon dioxide
PCA	phase contrast angiography
PCr	phosphocreatine
pH_e	extracellular pH
pH_i	intracellular pH
P_i	inorganic phosphate
pK	logarithmic acid dissociation constant
PWI	perfusion weighted imaging
RARE	rapid acquisition with relaxation enhancement
rCBF	regional cerebral blood flow
RCP	representative concentration pathway
ROI	region of interest
SNR	signal-to-noise-ratio
SST	sea surface temperature
T	Tesla, derived unit of magnetic induction
T_1	longitudinal relaxation time
T_{1A}	apparent T_1
T_2	transversal relaxation time
T_2^*	spin-spin-relaxation time
T_A	acquisition time
T_E	echo time
ToF	time of flight angiography
T_R	repetition time
µm	micrometre
δ	chemical shift
v	frequency
µatm	micro atmosphere

II. Figures

Figure 3-1 *In vivo* ^{31}P-NMR spectrum calibrated to PCr as 0 ppm illustrating the measurement of the chemical shift (δ) of Pi in relation to PCr. 9

Figure 4-1 Photo of a polar cod (*Boreogadus saida*) in its habitat (photo: Hauke Flores/AWI)..... 11

Figure 4-2 Technical drawing of the experimental setup. 12

Figure 4-3 Technical drawing of the in-house built experimental chamber. 14

Figure 4-4 Experimental chamber at the positioning device in front of the MRI. 14

Figure 4-5 Photo of the used MRI and positioning device. 15

Figure 4-6 Example of an axial FLASH scan in vivo with marked ROIs for the evaluation of blood flow. 18

Figure 5-1 Comparison of two different MR imaging techniques. 22

Figure 5-2 Morphological RARE MRI scans of the brain of polar cod. 22

Figure 5-3 Example axial FLASH scan of a Polar cod head. 23

Figure 5-4 3D Angiography MIP axial plane in anterior view. 24

Figure 5-5 3D Angiography MIP in the coronal plane dorsal view. 25

Figure 5-6 3D Angiography MIP sagittal plane. 25

Figure 5-7 example axial phase contrast imaging scans. 26

Figure 5-8 Axial phase contrast imaging scan of fish 6 with ROIs annotated in their respective position. 27

Figure 5-9 Time series of measured blood flow in ROI 1, ROI 2 and ROI 3 in fish 6. 28

Figure 5-10 Time series of measured blood flow in ROI 1, ROI 2 and ROI 3 in fish 7. 30

Figure 5-11 Time series of measured blood flow from phase contrast imaging in ROI 4, ROI 5 and ROI 6 in fish 7..... 31

Figure 5-12 FLASH axial MRI image annotated with ROIs of Polar cod (fish 6) in vivo 32

Figure 5-13 Time series of signal intensity from T_1-weigthed imaging in ROI 1-4 in fish 6. 33

Figure 5-14 Time series of measured signal from T_1-weigthed imaging intensity in ROI 1-4 in fish 7. 34

Figure 5-15 BOLD axial MRI image annotated with ROIs of Polar cod (fish 6) in vivo. 35

Figure 5-16 Time series - BOLD in vivo MRI scans of fish 6 in ROI 1- 4 in fish 7..... 37

Figure 5-17 BOLD axial MRI image annotated with ROIs of Polar cod (fish 7) in vivo. 38

Figure 5-18 Time series - BOLD in vivo MRI scans of fish 7 in ROI 1-3 in fish 7..... 39

Figure 5-19 Boxplots showing the P_i-PCr-ratio for fish 6 and fish 7 compared by experimental category (post handling, control, treatment, post treatment). 40

Figure 5-20 Boxplots showing the βATP signal intensity for Fish 6 and Fish 7 compared by category (post handling, control, treatment, post treatment). 41

Figure 5-21 Time series plots of the P_i-PCr-ratio (top) and βATP signal intensity in fish 6 over time. 42

Figure 5-22 Time series plots of the PI/PCr-ratio (top) and βATP concentration in fish 7 time. 43

Figure 5-23 Comparison of sum spectra of a fish after handling and after 18h post handling. 44

Figure 5-24 Time series of pHi from 31P NMR over the post-handling acclimation phase. 45

Figure 5-25 ^{31}P NMR sum spectrum showing a double peak around the δ of Pi. 45

Figure 5-26 Boxplots showing the intracellular pH (pH_i), calculated from chemical shift, for fish 6 and fish 7 compared by experimental category (post handling, control, treatment, post treatment). 46

Figure 5-27 Time series of the pH_i by condition. 47

Figure 10-1 Photo of a phantom solution injected into a sealed glass vial. The vial was positioned within an experimental chamber. 66

Figure 10-2 Titration curve..... 68

III. Tables

Table 1 Seawater alkalinity parameters..... 12

Table 2 measured chemical shifts of the ^{31}P-NMR spectroscopy phantom trials. 64

Table 3 chemical composition of the ^{31}P-NMR Spectroscopy phantoms..... 66

1 Executive summary

Polar cod (*Boreogadus saida*) is a key species of the arctic food web. It has a linking function between the trophic level of zooplankton and the top predators like marine mammals and seabirds. Under climate change and it shifts its distribution northwards and decreases in numbers. Under ocean acidification, by increased CO_2 accumulation, polar cod exhibits alterations in its neurochemical profile as well as behavioural alterations. The underlying factors are still poorly understood. In airbreathing vertebrates, increased concentrations of CO_2 (hypercapnia) leads to increased cerebral blood flow, so it was suggested that one of the underlying factors of those behavioural alterations might be accompanied by increased cerebral blood flow. Besides potential changes in the blood distribution, elevated environmental CO_2 might affect the acid-base status of the brain and its energy metabolism. Therefore, this study aimed to adapt an array of non-invasive magnetic resonance imaging (MRI) techniques to investigate potential changes in the blood distribution of the brain of polar cod under ocean acidification accompanied with measurements of the intracellular pH and energy status of the brain cells. To investigate blood flow, phase contrast MR imaging, FLASH MR imaging and BOLD imaging were adapted and successfully used under control conditions and conditions of elevated CO_2 concentrations in seawater. These investigations were complimented by *in vivo* ^{31}P-NMR spectroscopy to investigate potential changes in intracellular pH and energy metabolism. The presented study attained to deliver the first multi-parametric datasets, investigating blood supply on different levels of the vascular system of the head combined with observations of the acid-base and energy status of the brain of polar cod. Fluctuations in blood flow and perfusion were observed, but no significant elevation could be identified under ocean acidification. Ocean acidification induced decreases in intracellular pH were subtle and compensated for completely within 24 hours. No substantial alterations in the energy metabolism of the brain were detected under elevated CO_2. This study confirms previous work that found that the regulation of the acid-base status in the fish brain was fast and complete and advanced the current knowledge about the effects of ocean acidification on cerebral blood flow in fish. While previous works found showed that venous and arterial blood flow velocities in polar cod were decreasing under CO_2 this study did not find suspected CO_2 dependent blood flow alterations in the vasculature of the head.

2 Abstract

Polar cod (*Boreogadus saida*) is a key species of the arctic food web and links trophic levels. Under ocean acidification (OA), the accumulation of CO_2, polar cod exhibits neurochemical alterations as well as behavioural alterations. The underlying factors are still poorly understood. In airbreathing vertebrates, increased CO_2 concentrations (hypercapnia) cause increased cerebral blood flow (CBF). Besides potential changes in the blood distribution, elevated environmental CO_2 might affect the acid-base status of the brain and its energy metabolism. Therefore, this study aimed to adapt an array of *in vivo* magnetic resonance imaging (MRI) techniques to investigate potential changes in the blood distribution of the brain of polar cod under OA. To investigate blood flow, phase contrast MRI, FLASH MRI and BOLD imaging were adapted and used under control conditions and conditions of elevated CO_2 concentrations. These investigations were complimented by *in vivo* ^{31}P-NMR spectroscopy to investigate potential changes in intracellular pH and energy metabolism. Fluctuations in blood flow and perfusion were observed but no significant elevations could be identified under OA. OA induced decreases in intracellular pH were subtle and compensated for completely within 24 hours. No substantial alterations in the energy metabolism of the brain were detected under elevated CO_2.

3 Introduction & Aims

3.1 Ocean Warming and Acidification (OWA) and Ecological Consequences

The extensive burning of fossil fuels and the resulting emission of CO_2 and other greenhouse gases to the atmosphere have already caused warming of the earth, including the oceans. This warming will continue over the 21st century even though there are different predictions about its extent. This ocean warming will lead to rising sea levels due to thermal expansion and melting ice, decreased sea-ice extend and altered ocean circulations (IPCC 2013). The rising temperature poses threats to a broad variety of marine organisms and biota associated with the sea on all trophic levels. (Alexander et al. 2018). Not only form those organisms an integral part of the marine ecosystem and provide important, ecosystem services but also provide an essential part of the food security of many countries and societies. Fish for example accounted for 16.6 percent of the world's intake in animal protein in 2009 (FAO 2012). Especially in the Arctic Ocean physical and biological conditions are changing at unprecedented rates (Gaston *et al.* 2003, Polyakov *et al.* 2005). Physical factors such as an elevated SST and decreased sea ice coverage lead to serious shifts in the biogeography of fish stocks, their temporal and spatial distribution and abundance. (Gaston *et al.* 2003, Pörtner & Knust 2007, Pörtner *et al.* 2008) Additionally, to global warming, the oceans pH decreases by carbon dioxide (CO_2) intake from the atmosphere to the water. This process is known as ocean acidification (OA). CO_2 dissolves in the ocean and reacts with seawater in a process that forms carbonic acid. Hereby the ocean acidifies the partitioning of inorganic carbon shifts towards increased CO_2 and dissolved inorganic carbon and decreased carbonate ions concentrations. Ocean surface pH has already decreased by 0.1 units compared to pre-industrial times (Field *et al*. 2014). The further decrease in pH depends on both the future emissions of carbon dioxide and the emissions pathways (Representative Concentration Pathways (RCP)) as projected by the Intergovernmental Panel on Climate Change (IPCC) for the end of the century (IPCC 2013). Under unabated emissions ocean surface pH might decrease about 0.4 units compared to pre-industrial times by the end of the 21st century (Field *et al.* 2014, Gattuso *et al.* 2015). In the Arctic these alterations in pH and pCO_2 may even be stronger and faster due to the high solubility of gases in cold water (Fransson *et al*. 2009). The Representative Concentration Pathway (RCP) projects a sea surface temperature (SST) rise of 4 to 11 °C for the Arctic in the business-as-usual case (RCP 8.5, IPCC 2014) accompanied by a partial pressure of

carbon dioxide (pCO_2) rise from 400 µatm to 1370 µatm. High CO_2 levels affect marine biota on all trophic levels and has acute impacts on vital physiological functions and chronic impacts on vital aspects of their life cycles (Ishimatsu et al. 2005, Esbaugh 2018). Under high ambient pCO_2, CO_2 diffuses into animals via their epithelia decreasing first the extracellular pH (pH_e) and then in intracellular compartments. In tissue, the formation of carbonic acid is catalysed through carbonic anhydrase under hypercapnia. This facilitates a balance of acid-base equivalents, namely H^+ and HCO_3^- (Clairborne *et al.* 2002).

The effects of elevated CO_2 concentrations in sea water are diverse. Albeit a present lack of knowledge about the extent of the ecological consequences of high CO_2 concentrations in the world's oceans variety of effects were demonstrated. Elevated CO_2 concentrations will affect fish due acute, potentially lethal, effects on vital physiological functions as well as due to chronic, sublethal impacts on other aspects of their life cycle. Lethal pCO_2 appears to vary between species and especially early life stages are sensitive to high CO_2 (Ishimatsu *et al*. 2005)

Especially behavioural changes in a high CO_2 world are of interest as studies showed that certain species exhibit altered behaviour under simulated ocean acidification (Ishimatsu et al. 2005, Tresguerres & Hamilton 2017). Polar cod (*Boreogadus saida)* for example exhibits behavioural disturbances like significantly reduced absolute laterality and a shift in relative laterality under elevated CO_2 (Schmidt et al. 2017a). Also, neurochemical alterations in the brain of polar cod like an significant increase in GABA at high pCO_2 (Schmidt *et al.* 2017b). In Atlantic cod (*Gadus morhua*) studies could show strong aversive behaviour towards water with increased pCO_2 (Jutfelt & Hedgärde 2013). *In vivo* magnetic resonance imaging (MRI) and spectroscopy (NMR) studies revealed, that the acid base regulation in the brain is particularly affected under elevated CO_2 concentrations (Wermter *et al.* 2018). Active acid base regulation of the brain is an energy consuming process and appears to be limited in polar cod under OWA (Schmidt *et al.* 2017b).

3.2 Model species

In this study polar cod (*Boreogadus saida*) was used as model species. As being highly specialist to cold water and polar regions, polar cod is critically affected by ocean warming and acidification. Polar cod has its temperature range from -2 to +8°C. (Drost *et al*. 2014) and is regularly associated with sea ice. The are considered demersal or semi-pelagic with a strong surface orientation of eggs and larvae and an orientation to deeper habitats including demersal habitats at the end of their first year (Geoffroy *et al.* 2016). The distribution ranges of polar cod appear to have shifted northwards with decreasing numbers at the edges of their distribution and reduced numbers in years with reduced sea ice cover (Mueter *et al*. 2016). Recent studies predicted further habitat losses in polar cod under OA due to a narrowing of thermal ranges during the embryonic development (Dahlke *et al*. 2018) and behavioural alterations (Schmidt *et al.* 2017a). Kunz *et al.* (2018) demonstrated that polar cod possesses reduced maximum swimming capacity after long time acclimation to future OAW conditions (RCP 8.5 scenario, IPCC 2014) even though they could not find significant differences in standard metabolic rate. The linking function of polar cod among trophic levels in the Arctic food web is at stake if the standing stock shifts its distribution further northwards, which might result in cascading ecological consequences. To be able to project ecosystem impacts caused by climate change, the assessment of tolerance ranges and acclimation capacities of key species is crucial (Kunz *et al.* 2018). Its predicted that under the predicted OWA scenarios Polar cod will show shifts in populations abundances and los crucial parts of its spawning grounds (Dahlke *et al*. 2018). However, the underlying physiological factors that cause behavioural alterations are not well understood and there appears to be a knowledge gap. Possible factors like brain perfusion, alterations in the brain’s energy metabolism need further investigation.

3.3 Cellular energy metabolism, acid-base regulation, intracellular pH

Energy provision and consumption in fish is generally dependent on the levels and variability of activity and environmental factors. Different pathways contribute to the functional capacities if cells, organs and the whole organism. Energy demanding processes like ventilation, cardiovascular performance and acid-base regulation need to be fuelled.

In the cellular energy metabolism, adenosine tri-phosphate (ATP) is the most important nucleoside phosphate in the energy pathway. Biological functions from the generation of mechanical work to the powering of ion-transporters is fuelled by metabolic energy in form of ATP. As in most vertebrates, in fish, more than 95% of the ATP required in the cell metabolism under resting conditions is derived from the aerobic metabolism based in mitochondria, i.e. oxidative phosphorylation.

In fish, there are two main anaerobic pathways produce ATP in fish when there is high availability of energy. The more relevant here is PCr hydrolysis following the formula:

$$\text{creatine} + \text{ATP} \rightarrow \text{phosphocreatine} + \text{ADP} + \text{H}^+$$

Under conditions of rapidly increasing energy demand or when oxygen is limited this process is reversed using PCr as store of high-energy phosphates that are easily and timely assessable. PCr can donate phosphates to ADP forming ATP. PCr as energy store allows fast energy transfer to ATP at rates far higher than by aerobic or anaerobic metabolism. As it is the first energy source to be used under high energy demand such as burst swimming it is used under handling stress, anoxia and possibly hypercapnia (Borger et al. 1998). The signal intensity of inorganic phosphates (Pi) rises with increased energy demand. In teleosts, PCr levels are typically high in energy demanding tissues like skeletal muscle and nervous tissue and low in other organs. This allows its use in ^{31}P NMR spectroscopy studies of the energy metabolism of muscles and brain.

Fish must maintain homeostasis of their intra- and extracellular pH like other vertebrates but face constraint due to the aquatic environment they are living in (Clairborne *et al*. 2002). Under normal conditions pH is tightly controlled in organisms due to its critical role for the function of cellular processes such as the energy metabolism. While the measurement of blood pH (i.e. extracellular pH (pHe)) is relatively simple, the accurate measurement of intracellular pH (pHe) in vivo is more challenging.

3.4 Blood distribution

One of the permanent tasks of blood is to provide the gas exchange, i.e. O_2-transportation from the respiratory organs (e.g. gills) to the tissues where it is needed

and in turn the removal of CO_2. This is the case for all animals except *Tracheata*. In the respiratory organs, i.e. lungs and gills, O_2 is incorporated and then distributed in the body by energy consuming processes like the heartbeat. The heart pumps the blood through arteries and from there through their smaller branches, the arterioles, and finally trough the capillaries. Capillaries, small blood vessel from 5 to 10 µm in diameter, forming a fine mesh, the capillary bed, where the actual exchange of gas and nutrients between the blood and the tissues happens. After the capillaries, the blood is transported by venules and veins back to the heart. This is true for those animals having a closed circulation system including vertebrates (Soldatov 2006). Cartilaginous and bony fish are the first groups of organisms whose capillary networks are close to those of terrestrial vertebrates. They differ though in in reactivity of vessels to vasoactive compounds and ecological factors and show a heterogeneity of vessels in the capillary bed and a permeability of capillary units to organic compounds different to other vertebrates (Söderström & Nilsson 2000).

In vivo cardiac responses to hypercapnia vary amongst fish species. Similarly, corresponding blood pressure responses vary amongst species. Bradycardia appears to be a common but not universal response to hypercapnia among teleosts (Perry & Gilmour 2006). In rainbow trout (*Oncorhynchus mykiss*), direct vasodilatory effects of elevated pCO_2 on the peripheral vasculature were found (Mckendry and Perry 2001). Other studies showed increased blood pressure in different species due to peripheral vasoconstriction. There appears to be no obvious pattern across teleost species (see Perry & Gilmour 2006 for review). In Atlantic cod (*Gadus morhua*), reduced cardiac output could be shown under severe hypercapnia (Gesser & Poupa 1983). Also, the contractile force in the myocardium of *G. morhua* has been shown to decrease under high CO_2 to an extend lower than of compared species (Gesser & Jørgensen 1982). Schmidt (2019) showed significantly lowered arterial and venous blood flow both in polar cod under increased CO_2 (1668 ± 250 µatm)) and normal blood flow was not restored within the observation period of four days.

Perfusion is defined as the passage of blood through an organ's vascular network, e.g. the microcirculation trough the capillary bed of the brain. Perfusion can be assessed non-invasively by MRI measurements of cerebral blood flow (CBF), cerebral blood volume (CBV) and mean transit time (MTT). In mammals and other air breathing vertebrates, e.g. turtles, hypercapnia causes cerebral vasodilation which leads to

increased CBF (Bickler 1992, Buchanan & Phillis 1993, Duelli & Kuschinsky 1993). Currently there is poor knowledge about the regulation of cerebral blood flow (CBF) in fish and other “lower” vertebrates.

3.5 Magnetic Resonance Imaging (MRI)

In vivo magnetic resonance imaging (MRI) allows to study physiologic processes non-invasively in a living organism. MRI bears the advantages to allow scans of soft tissue (other than other imaging modalities like x-ray) and allows the measurement of flowing liquids (e.g. diffusion and perfusion) in a living organism, both physiologic and pathologic. Furthermore, MRI allows the characterization and discrimination among tissues using their physical and biochemical properties (water, iron, fat, and extravascular blood and its breakdown products). It provides three-dimensional non-invasive quantitative methods of cerebral blood flow (CBF) quantification.

Specific parameters were introduced for an understanding and characterisation of MR imaging contrast. In particular, the T_1 relaxation time, also known as spin-lattice relaxation time, describes the time net magnetisation vector of an excited particles spin recovers to its ground state according with B_0. T_1-weighted imaging is frequently applied for separation of tissues by differences in image contrast, which depends on the different T1 relaxation times of different tissues. T_2-relaxation-time describes the spin-spin-relaxation time. This refers to the progressive dephasing of the spin of the nuclei after the end of a 90° pulse. The time this dephasing takes is tissue-dependent. T_2 is long in pure water and comparably faster in macromolecules and tissues. T_2*-weighted imaging is a MRI sequence used to quantify effective T_2*, which depends in addition to T_2 on local changes in the magnetic field homogeneity caused by minor differences in the chemical environment. T_2*-weighting is therefore used for functional imaging.

T_1-weighted MR imaging (FLASH)

T_1-weighted is a method advised for stationary anatomical applications. T_1-weighted imaging is usually achieved using a gradient echo method (e.g. fast low angle shot (FLASH) or spin-echo sequence (such as Relaxation Enhancement (RARE) MR imaging) with a short repetition time (T_R) (Matthaei *et al.* 1985). T_1-weighted imaging methods exhibit a high signal intensity for fat, fatty bone marrow, paramagnetic contrast agents and slow flowing blood. The sensitivity for slow flowing blood makes it a method of particular interest for this study. FLASH methods allow the acquisition of time courses.

Blood oxygenation level dependent (BOLD) MR imaging

Blood oxygenation level dependent (BOLD) imaging is a T_2*-weighted gradient echo method to generate images to assess differences in the ratio of oxygenated and deoxygenated blood (Ogawa *et al.* 1990). Oxygenated haemoglobin is diamagnetic and deoxygenated haemoglobin is paramagnetic. Paramagnetic materials induce changes in T_2* values of tissues, therefore changes in oxygenated and deoxygenated ratio of blood can be followed up with this technique and is frequently used in functional MRI (fMRI) and resting state MRI.

Flow-weighted MR imaging

Flow-weighted MR imaging is a flow-compensated gradient echo method and is frequently used for the quantification of blood flow changes in vessels (Underwood *et al.* 1987). Classic applications of the phase contrast imaging are angiography and the observation of blood flow changes. The analysis of the MR phase signal allows the quantitative mapping of blood velocity in heart and large vessels.

3.6 ^{31}P-NMR Spectroscopy

Nuclear Magnetic Resonance (NMR) spectroscopy is one of the most established platforms to analyse the composition of substances and is nowadays used in

metabolomics. *In vivo* ^{31}P-NMR spectroscopy has been popular since 1973 to detect high energy phosphates such as ATP and its end product, inorganic phosphate, which can be used to estimate the intracellular pH *in vivo* (Beirnaert *et al.* 2018, Roberts *et al.* 1981).

The chemical shift (δ) of the inorganic phosphate (Pi) NMR signal is sensitive to changes in pH within the physiological range and many studies have been published on the calibration of pH in ^{31}P-NMR spectroscopy in brain, other organs and tissues (e.g. Kost 1990). For pH estimation from ^{31}P-NMR spectra standards are needed. The chemical shift of a certain molecule can either be compared to an external standard like Methylenediphosphat (MDP) or to an internal standard. In this study phosphocreatine (PCr) was used as internal standard as its chemical shift is not pH dependent (Kost 1990). Measurement of chemical shift of the centre of the resonance line in the sample towards the internal reference standard phospocreatine can be represented by the following formula with the peak at the resonance frequency of PCr as ν_{ref} and the peak at the resonance frequency of Pi as ν_{sample}.

$$\delta = \frac{\nu_{sample} - \nu_{ref}}{\nu_{ref}}$$

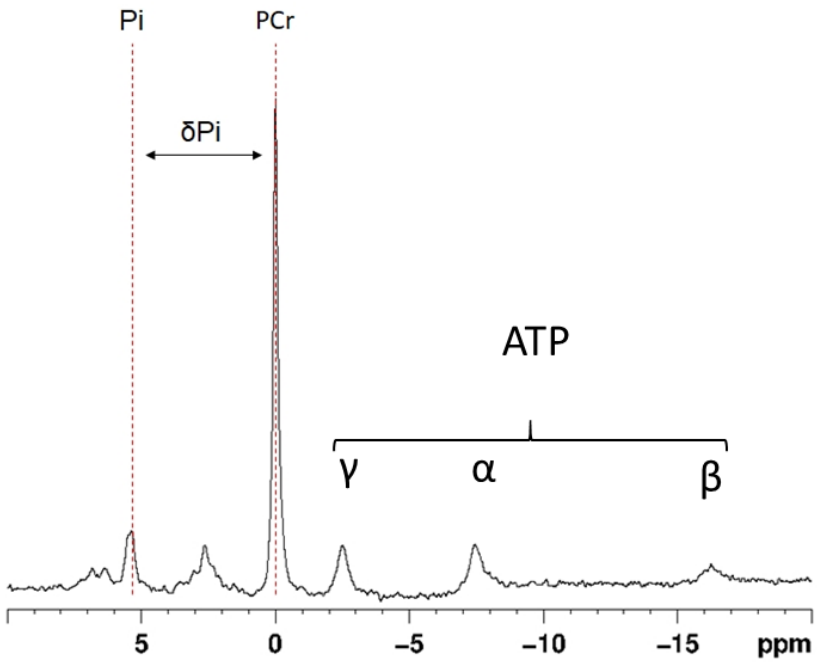

Figure 3-1 *In vivo* ^{31}P-NMR spectrum calibrated to PCr as 0 ppm illustrating the measurement of the chemical shift (δ) of Pi in relation to PCr.

As the pH-value of the second proton dissociation of the inorganic phosphate is close to neutrality the measured chemical shift of Pi can be transformed into a pH. Under *in vivo* conditions, this signal is mostly representing the intracellular milieu and is therefore transformable into an intracellular pH (pHi). To derive the pHi, from observed chemical shifts (δo), the logarithmic acid dissociation constant (pK) is needed as well as the chemical shift of the acid (δmin) and the chemical shift of the base (δmax) from a calibration curve. Using these values and a modified Henderson-Hasselbalch equation for a single equilibrium the pH can be calculated (Roberts *et al.* 1981).

$$\mathrm{pH} = \mathrm{pK} + \log\left[\frac{\delta\mathrm{max} - \delta\mathrm{o}}{\delta\mathrm{o} - \delta\mathrm{min}}\right]$$

Reference measurements were performed using artificial phantoms with defined pH-values in the relevant physiologic pH-spectrum ranging at levels from pH 6.8 up to 8 to create a titration curve for the calibration of following *in vivo* measurements.

3.7 Aims

The main aim of this work was to adapt a set of non-invasive methods to investigate possible neurophysiological effects of ocean acidification in the brain of polar cod. Possible alterations in the blood supply of the brain, potentially due to vasodilation under hypercapnia, shall be assessed. To investigate this question MR imaging methods used in medicine and basic pre-clinical research were adapted for the use in marine polar fish.

Simultaneously, a protocol should be delivered to assess blood supply and alterations in the brain's energy metabolism and acid-base status. Therefore, an *in vivo* ^{31}P NMR spectroscopy protocol was applied additionally to the MR imaging

The experimental protocol was tested to investigate potential physiological effects in the brain of polar cod to acute changes to ocean acidification.

4 Materials & Methods

4.1 Specimens and animal maintenance

In this study polar cod (*Boreogadus saida*) were used as model animal. N=7 animals ranging from 19-26 cm total length and weighting between 26 and 63 g were used in this study. The fish were caught 2018 during deep water trawls using a fish lift onboard the RV 'Heincke' by the Alfred Wegener Institute in the Billefjord, Svalbard, at temperatures between -1° C and -1.5° C in depths between 130 m and 190 m (RV Heincke Cruise HE519 (DOD-Ref-No.20180069, Mark 2018)). The fish were transported to the AWI and held in the section´s aquarium facility in tanks supplied with natural seawater at 0°C and were fed once a week with frozen shrimp and mussels.

Figure 4-1 Photo of a polar cod (*Boreogadus saida*) in its habitat (photo: Hauke Flores/AWI).

All procedures were approved in accordance with the regulations for the welfare of experimental animals issued by the Federal Government of Germany (§11 Abs. Ziff. 1 a+b) AZ: 0515_2040_15 and with the guidelines of the European Union (2010/63/EU) for care and use of laboratory animals.

4.2 Water supply and seawater chemistry

The water supply is based on a water reservoir tank (i.e. header tank) that was stored high to achieve a gravity-based/hydrostatic water flow through the chamber. The water in the storage tank was cooled to a defined temperature of 0.5° C by thermostats and was enriched with a controlled gas mixture. There were two header tanks (50 L each), one supplied with an atmospheric gas mixture as control condition and the second with an elevated pCO_2 gas mixture. The connection tubing between the tanks and the chamber could be switched at any time and allowed an acute change in treatment without a ramp up. A constant water flow of about 500 ml/min was set. After flowing through the chamber, the water was be pumped back to the storage tank with a peristaltic pump (Masterflex I/P Easyload model 7529-10), cooled and enriched with gas again.

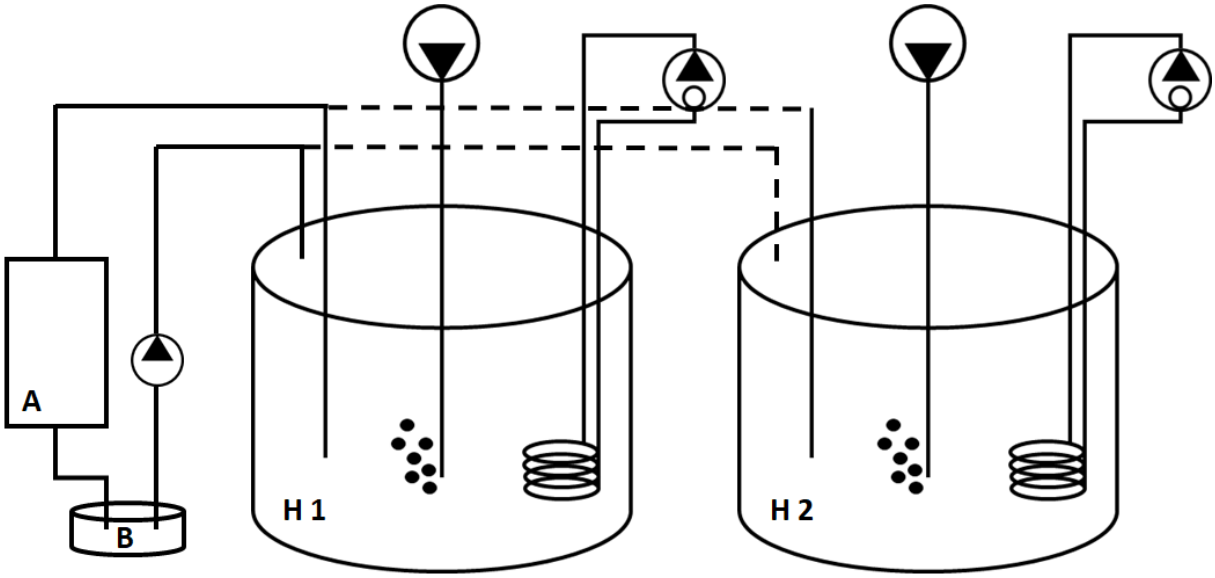

Figure 4-2 Technical drawing of the experimental setup.
The experimental chamber as a flow-through chamber (A), flow through tank were flow can be measured and adjusted (B), the two header tanks (H1 seawater at atmospheric pCO_2, and H2 at elevated pCO_2) (adapted after Wermter et al. 2018).

The setup and control of the seawater chemistry under conditions of ocean acidification was designed according to the 'Guide to best practices for ocean acidification research and data reporting' (Riebesell et al. 2011). The seawater alkalinity was calculated using CO2Sys_v2.1.xls (Pierrot *et al.* 2006).

Table 1 Seawater alkalinity parameters

condition	T [°C]	Salinity [psu]	pH (NBS) Seawater	pH (NBS) Dickson	pCO_2 [ppm]	pH total scale	pH freescale
control	0.5	30.4	8.01	8.8	517.7	8.102	8.143
treatment	0.5	30.3	6.94	8.8	3482.1	7.032	7.073

Temperature was measured online simultaneously in both header tanks (H1 and H2) and in the tubing at the exit of the experimental chamber using glass fibre optical thermometer (i.e. optode) (OPTOCON AG, Optical Sensors and Systems, Dresden, Germany). The temperature regulation was achieved by cooling the header tanks and insulation of all tanks and tubing. The header tanks were cooled using cooling thermostats (LAUDA, RC 6 CS and ECO RE 630). Salinity in the header tanks was controlled repeatedly using a conductivity-meter (WTW LF197). The pH as controlled repeatedly measuring the total hydrogen concentration using a pH meter (WTW, profiline pH 3310) calibrated with two defined calibration solutions and a Dickson tris buffer as reference. Gas was supplied in form of compressed air and concentrated CO_2 from an in-house centralized gas supply system. Gas was mixed by a mass-flow controller (mks Instruments Deutschland GmbH, PR 4000) before being pump into the header tanks and being diffused by airstones. The respective pCO_2 in the treatment seawater tank was controlled repeatedly using a Vaisala CARBOCAP carbon dioxide probe GMP343 coupled with a Vaisala relative humidity and temperature probe.

4.3 Experimental setup and protocol

The handling of the animals prior experimentation followed a strict protocol. One animal was retrieved from the aquarium facility prior to the experiment (with one person assisting) and fish was transferred to an in-house built experimental chamber made from polyurethane within the cooled aquarium facility. The chamber consisted of a main part with two hose connections for seawater inflow and outflow and a positioner to adapt the free space within the chamber to the fish's length. The bottom and sides of the frontal part of the chamber was coated with dental wax additionally to adjust for the curvature of the fish. After transportation to the NMR laboratory the chamber was

closed and it was connected to the seawater cycle. The closed chamber was attached to a positioning device and inserted into the centre of the magnet (see Figure 4-4).

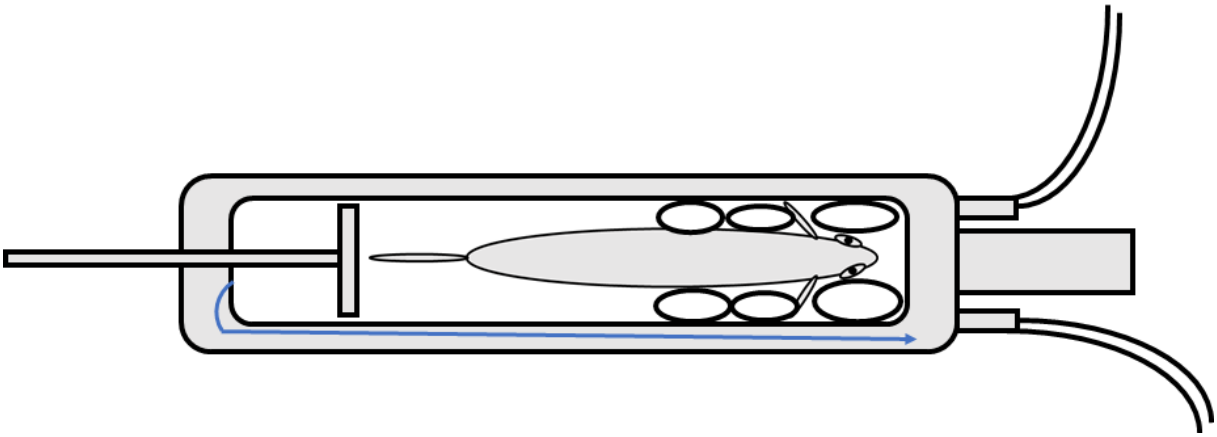

Figure 4-3 Technical drawing of the in-house built experimental chamber.
The chamber is equipped with a positioner and dental wax to modulate for the size and shape of the individual fish for scanning. At the right end of the chamber two hose connecters allow the connection of the chamber to the respective seawater cycle. The blue arrow indicates the outflow of seawater from the chamber.

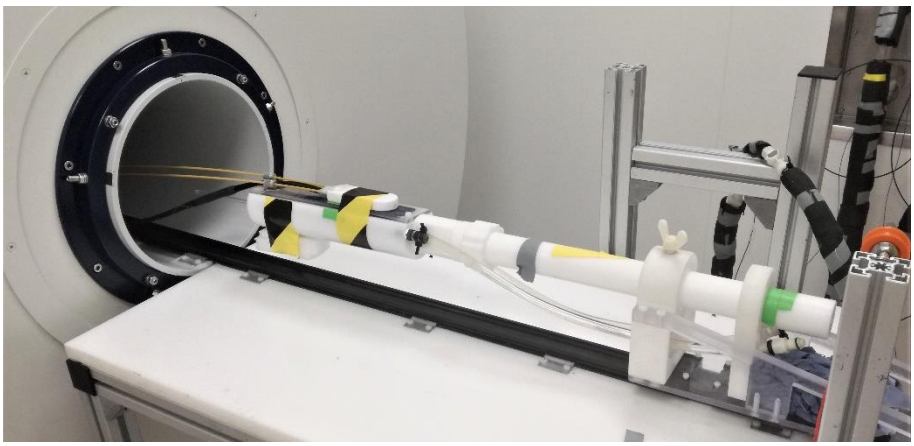

Figure 4-4 Experimental chamber at the positioning device in front of the MRI.
The ^{31}P-NMR surface coil was attached to the upper side of the chamber. The chamber is connected to the seawater cycle by hoses.

4.4 Nuclear magnetic resonance imaging and spectroscopy

In vivo MRI and ^{31}P NMR spectra were obtained using a 9,4 T animal scanner with a horizontally accessible bore of 30 cm (Bruker Biospin MRI GmbH Ettlingen, Germany, BioSpec 94/30 US/R, AVANCE III) and a BGA-12S HP B_0 gradient system. The signal of the fish was collected with a 2 cm diameter surface coil which was double-tuned for the hydrogen and phosphorous frequencies. The NMR control software (Paravision 6.0.1, Bruker Biospin MRI GmbH) was run on a HP workstation with a Linux based operating system.

Figure 4-5 Photo of the used MRI and positioning device.
94/30 US/R, AVANCE III and in-house built positioning device and insulating tubing for the seawater supply.

4.4.1 Experimental protocol

The experimental chamber was placed into the centre of the MR scanner and the fish was allowed to acclimate to its new setting for 18 hours at least. After control of the position of the animal chamber inside the magnet, consecutive in vivo 31P-NMR spectroscopy scans were conducted over the time course of this post handling phase to control the acid-base and energy status for potential handling-induced alterations. After an acclimation phase the experimental protocol was started when the fish was considered free of handling stress. Treatment conditions were induced acutely for 24 hours to investigate potential changes in blood distribution, pH_i and energetic status of

brain cells. Finally, after the treatment a control phase of 3 hours was conducted under control conditions. Animals were transported back to the aquaria after the experiment. All animals survived the MR experiments except for one individual, due to an accidental stop in the water supply during the night.

Over a pre-treatment control phase of 3 hours, the treatment period and a post-treatment control phase of 3 hours *in vivo* ^{31}P NMR spectroscopy was performed as well as MR imaging. After a tri-pilot scan blocks of three consecutive spectra were followed by a FLASH scan, a BOLD scan and a phase contrast imaging scan. This scheme was repeated over the whole course of the control and treatment phase.

4.4.2 MR imaging and spectroscopy protocol

For the localization of the relevant field of view and for the verification of the fish's position within the chamber tri-pilot localizer scans were performed to generate an simple MR image giving an 3D overview. The used tri-pilot scans were based on the Bruker Localizer_Service protocol and slightly adapted. For each tri-pilot one scan was conducted with a T_E of 4.0 ms and a T_R of 100 ms which gave a fast T_A of 12 s 800 ms. The slice thickness was 2.0 mm at an image size of 128 x 128 pixels and a field of view of 80 x 80 mm. The excitation pulse was of 1.40 ms length and had a bandwidth of 3000.0 Hz at a FA of 30° and a power of 0.76 W.

The Bruker protocol FLOWMAP was used as base with the reconstruction mode "VelocityMapping". The used parameters were a T_R of 9.0 ms at T_E of 4.0 ms with a F_A of 20° gave a T_A of 1m 13s 728 ms duration for one slice and a field of view of 40 x 40 mm and 256 x 256 pixels. 16 averages were generated per scan and anti-aliasing was set to 1.0. The velocity range was set to its minimum of 4.49 cm/s. The excitation pulse used had a length of 0.78 ms, a bandwidth of 5400.0 Hz and a flip angle of 20°and 1.30 W power. Masking threshold was set to 0.0 % after exploratory scans showed very low signal intensities which would make the blood flow in blood vessels masked even under thresholds as low as 0.1 % signal intensity.

RARE scans were used for morphological investigations. The used examination parameters were T_R of 1000.0 ms and T_E of 40.0 ms and a 90° F_A. Eight averages

were obtained for one slice with a thickness of 1 mm per scan. A field of view of 40 x 40 mm and 256 x 256 pixels were obtained. T_A was 2 min 15 s 130 ms.

FLASH scans were used after modifications of the examination parameters to a T_R of 85.3 ms. For scans of 0.50 mm slice thickness and 16 averages per scan the T_E was set to 10.0 ms with a F_A to 60° generated suitable images for morphological analysis and verification of the position of the animal and identification of blood vessels. The acquisition time (T_A) was 6 min 33 s 238 ms for a scan with 6. The image size was 256 x 256 pixel for a field of view of 40.0 x 40 mm. The used excitation pulses had a length of 2.0 ms with a bandwidth of 4000 Hz and had a power of 6.45W.

To investigate possible differences in perfusion BOLD MRI scans were used. The used scanning protocol was based on the Bruker T1_FLASH. The parameters used were T_E of 40.0 ms, T_R of 100.0 ms with 16 averages resulting in a T_A of 7m 40 s 800 ms. For one slice with an image size of 256 x 256 pixels and a field of view of 40.0 x 40.0 mm. The excitation pulse had a length of 2.0 ms with a bandwidth of 4000.0 Hz and a FA of 60° and a power of 6.45 W.

^{31}P NMR spectroscopy parameters were as follows. The total acquisition time per 31P-NMR spectrum was = 5 min 07 s 200 ms. 256 scans/averages were conducted with a T_R of 1200 ms, a F_A of 65° and an acquisition duration of 409.6 ms. 4096 acquisition points were used at a acquisition bandwidth of 10000 Hz = 61.70 ppm, a spectral resolution of 1.22 Hz/points and the reference power was 2.714 W. The excitation pulses were bp32 (block pulses) with a length of 0.2 ms, a bandwidth of 6400 Hz and a pulse power of 16.96 W.

4.4.3 Image Analysis

Image analysis was performed in Paravision 6.0.1 (Bruker Biospin MRI GmbH) for phase contrast imaging and in FIJI is just ImageJ (Version 1.52n) for FLASH imaging, BOLD imaging. 3D MIPs were created in HOROS medical image viewer. In the

obtained MR images regions of interests (ROI) were evaluated either for signal intensity (BOLD and FLASH) or for flow velocity (phase contrast imaging).

In phase contrast imaging, if the position allowed at least three ROIs were chosen to measure the blood flow in brain vessels while the remaining ROIs were positioned to control for possible aliasing and movement artefacts. They were positioned in areas of the image that represented body tissue, water flow in the surrounding chamber, air outside the chamber and they were positioned according to phase gradient errors due to movement.

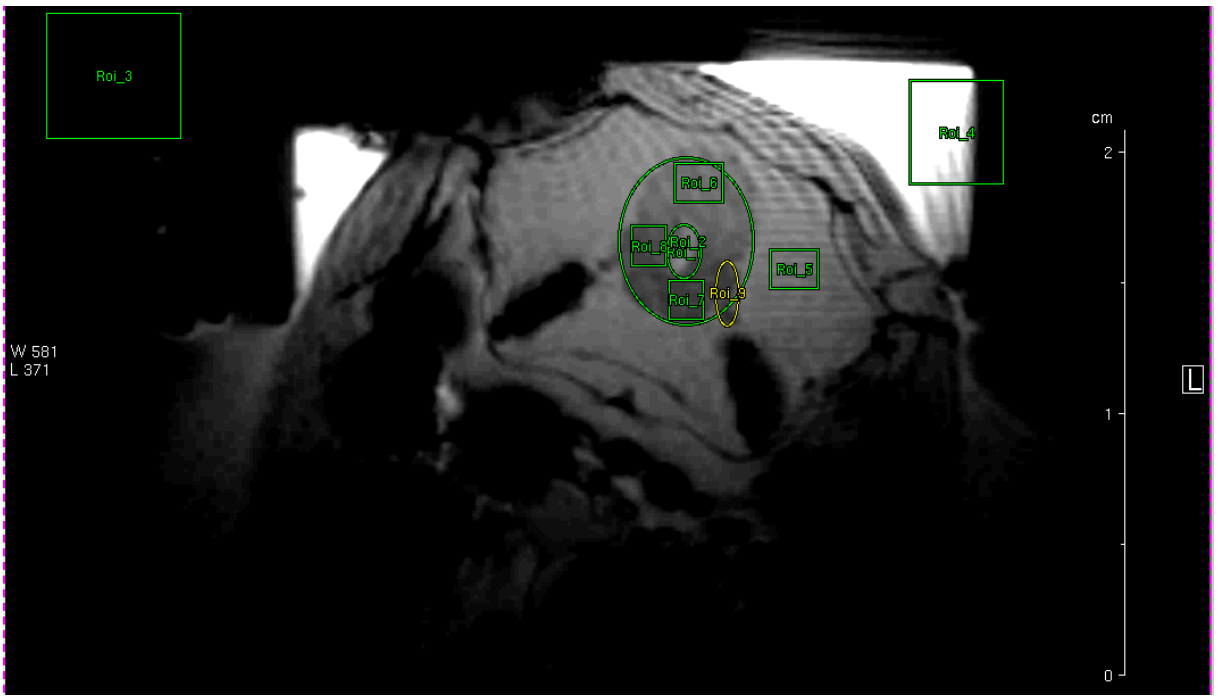

Figure 4-6 Example of an axial FLASH scan in vivo with marked ROIs for the evaluation of blood flow.

The NMR spectroscopy analysis workflow consist of several pre-processing steps including a conversion of the free induction decay (FID) to a spectrum in the intensity vs ppm format using a Fourier-transformation in Topspin 3.1PV (Bruker Biospoin GmbH), an automated baseline correction, and manual phase correction. The received

spectra were calibrated with the peak of PCr to 0 ppm as reference. All *in vivo* and *in vitro* calibration spectra were analysed manually.

As indices for the energetic status of the cell metabolism the P_i-PCr-ratio (ratio of the concentration of inorganic phosphate to phosphocreatine) was calculated as well as the signal intensity of βATP which is representative for the ATP level (Borger *et al*. 1998, van den Thillart 1989).

4.4.4 Statistical analysis

The data was exported and stored in Microsoft Office 365 Excel sheets. Statistical analysis was carried out using the software R version 3.5.3 (R Core Team, 2019). Images were obtained, stored and worked on as DICOM (Digital Imaging and Communications in Medicine) files. ^{31}P-NMR spectra were obtained and evaluated using Topspin Software for Paravision 6.0.1. (Bruker Biospin MRI GmbH).

5 Results

An experimental protocol was developed to investigate the effects of ocean acidification on the blood distribution and energy metabolism of the brain as well as its intracellular pH (pH_i) in Polar cod. The used scanning methodology was refined using a total of 5 fish and applied for experimentation on 2 fish under trial conditions. Different methodologies were tested and compared to investigate the blood distribution of the brain.

5.1 Brain morphology

A series of *in vivo* morphological scans were conducted on all animals (n = 7). Over the course of this work several MR imaging techniques were tried and compared to produce high quality *in vivo* MRI brain scans in Polar cod under control and treatment conditions. Different imaging techniques were tried and adapted. Rapid Acquisition with Relaxation Enhancement (RARE) MRI as well as Fast Low Angle Shot (FLASH) MRI scans were tried and compared for morphological imaging. The RARE imaging provided relatively high image contrasts and allowed discrimination between brain regions and surrounding tissues and even between different structures within brain areas. The RARE imaging did not allow the detection of blood flow or blood vessels. The FLASH imaging in contrast did not provide high contrast and was not very suitable for the discrimination of brain areas and tissues but did exhibit very strong signals even for small blood flows and was therefore suitable to detect blood vessels in the head of the fish and explore the heads vascularity (see Figure 5-1).

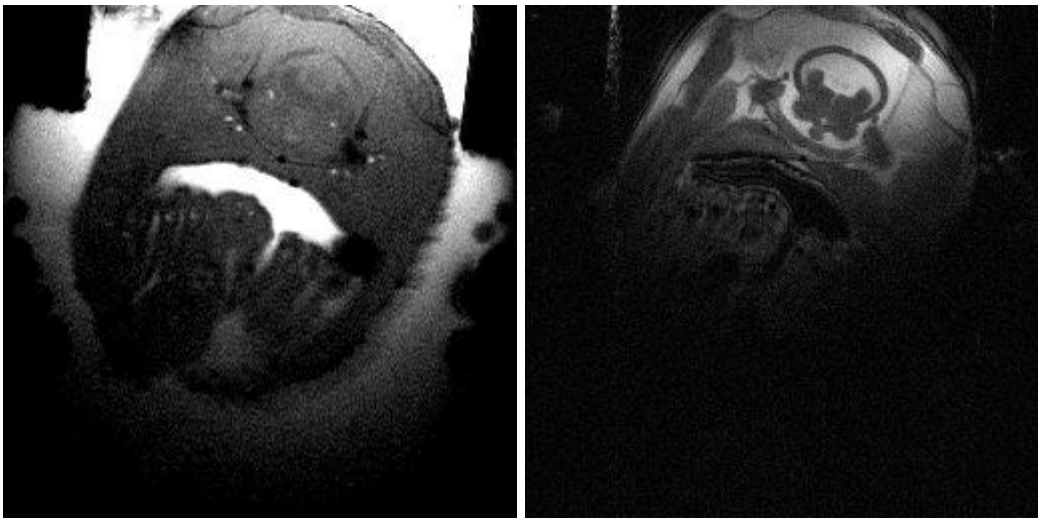

Figure 5-1 Comparison of two different MR imaging techniques.
On the left, there is a FLASH image. On the right there is a RARE image presented. Both images show axial scans (at the same position) through the head of the fish. The images show cross-sections through the fish's head. In the left image (FLASH) flow is displayed brightly exhibiting water filled mouth cavity and blood flow in the blood vessels of the head, around the brain and around the otoliths, as well as in the gills. In the right image (RARE) the different anatomical structures in the fish's head can be discriminated by contrast.

Figure 5-2 presents different morphological MR imaging views to illustrate the brain anatomy of Polar cod. Morphological scans of the fishes' brains and the surrounding head were obtained for the three planes and at different positions.

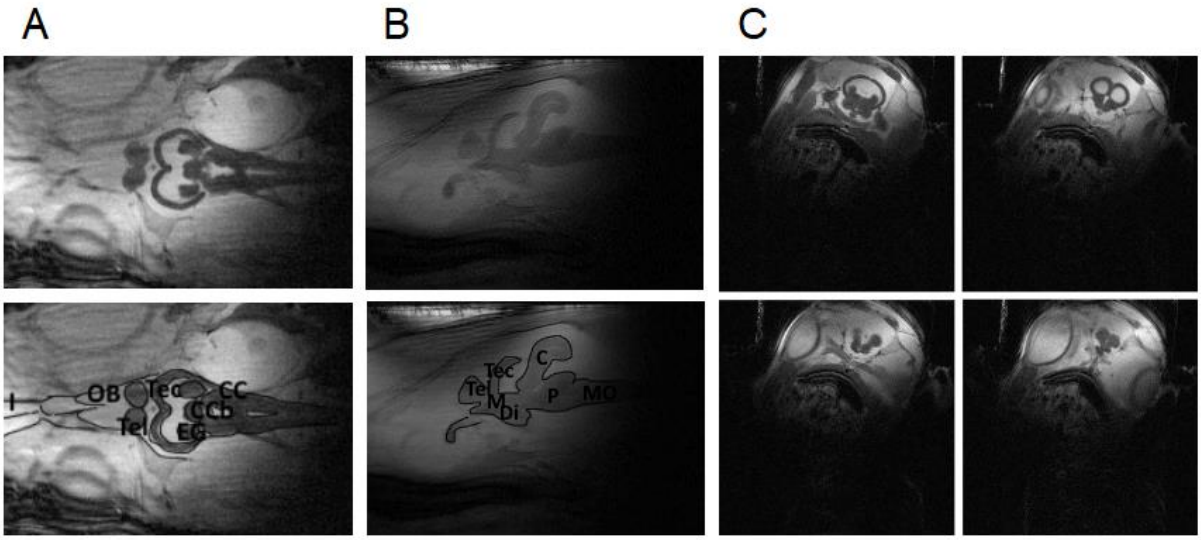

Figure 5-2 Morphological RARE MRI scans of the brain of polar cod.
(A) coronal plane (B) sagittal plane (C) axial planes at four different positions of the head. The annotated brain regions are I – olfactory nerve, OB – olfactory bulb, Tel - telencephalon, Tec – tectum, EG – eminentia granularis division of the cerebellum, Tel – telencephalon, M – mesencephalon, Di-diencephalon, P – pons, MO – medulla oblongata, CCb –corpus division of the cerebellum, C – Cerebellum. CC – crista cerebellaris of the rhombencephalon

5.2 Blood Flow and Perfusion

5.2.1 Vascular morphology

To investigate possible changes in brain perfusion under elevated pCO_2 *in vivo* suitable blood vessels for blood flow investigations had to be found. To find these vessels axial, sagittal and coronal scans were performed. To describe the morphology, distribution of these vessels in the fish head a 3D reconstruction was achieved. Axial scans were used in experiments to find vessels for further investigation using flow-weighted and BOLD MRI techniques.

5.2.2 Angiography scans

Serial axial T1_Flash scans were conducted over the whole length of the animal´s head to find and trace suitable blood vessels for perfusion weighted imaging. For every block of flow-weighted scans T_1- weighted scans were repeated to allow the identification of movement and repositioning of the fish.

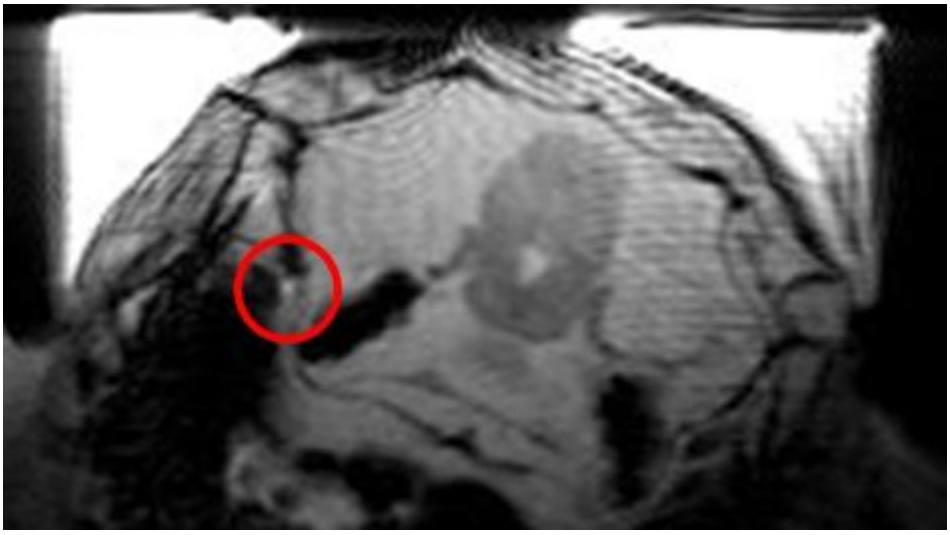

Figure 5-3 Example axial FLASH scan of a Polar cod head.
The image shos a cross-section of the fish head. Obtained for the localisation of blood vessel and neuroanatomical overview. Marked with a red circle a blood vessel is visible as a bright structure.

5.2.2.1 Angiography – Maximum intensity projection (*MIP*)

For one animal an 3-dimensional angiography model was rendered based on 40 separate time of flight (ToF) angiography scans to display and trace the blood vessels

of the fish's head. As the model is a maximum intensity projection (MIP) blood vessels cannot only be visualized by their signal intensity but also can flow within these be compared by signal intensity representing flow speed with an opacity following a linear table (see Figure 5-4 ff). Movie files of the 3D rendered angiography scans can be found in the digital annex.

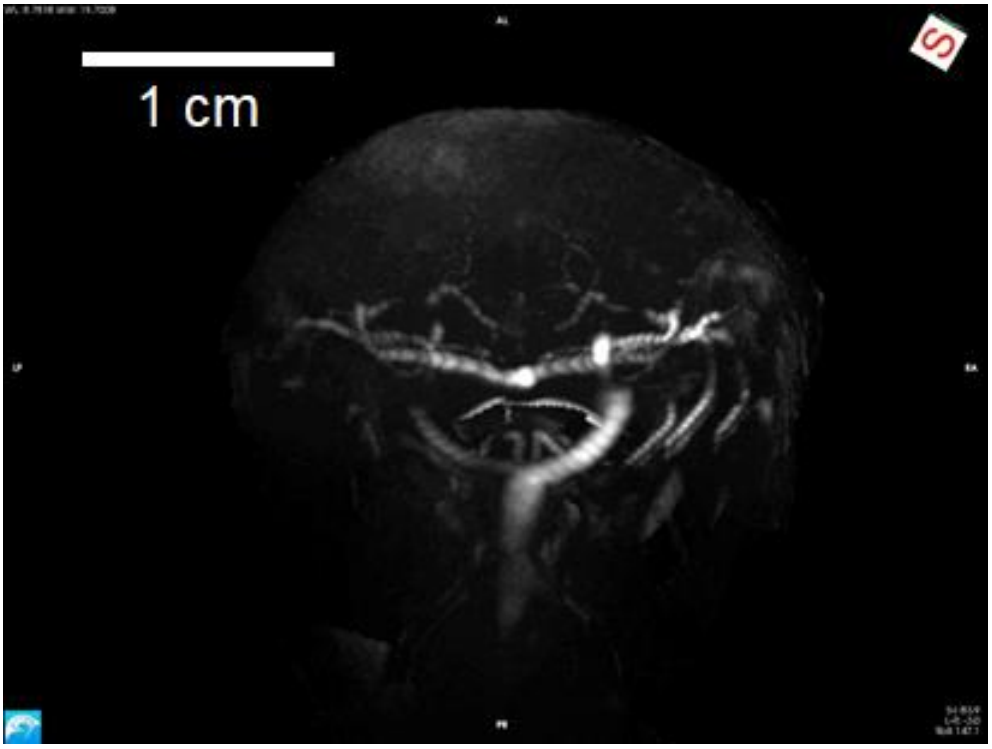

Figure 5-4 3D Angiography MIP axial plane in anterior view.
The 3D model is showing the blood vessels in the fish head. The upper side of the image is dorsal, the lower side ventral. The bright structures are the blood vessels in the head of polar cod. The mouth cavity and the gills were removed digitally.

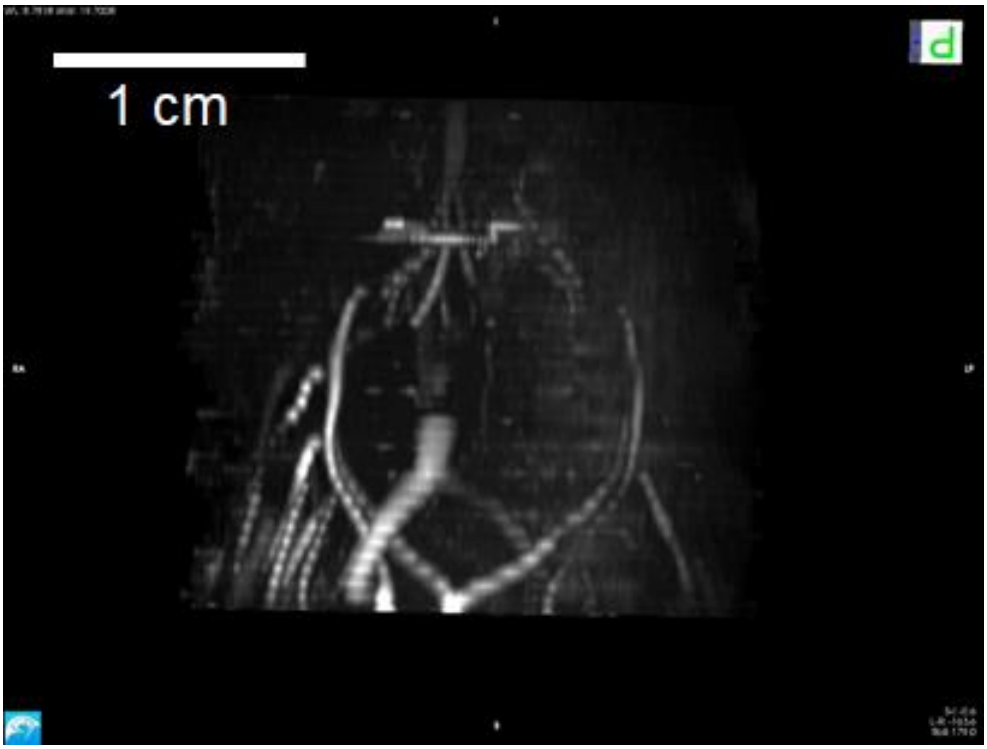

Figure 5-5 3D Angiography MIP in the coronal plane dorsal view.
The 3D model is showing the blood vessels in the fish head. The upper side of the image is caudal, the lower side ventral. The bright structures are the blood vessels in the head of polar cod. The mouth cavity and the gills were removed digitally.

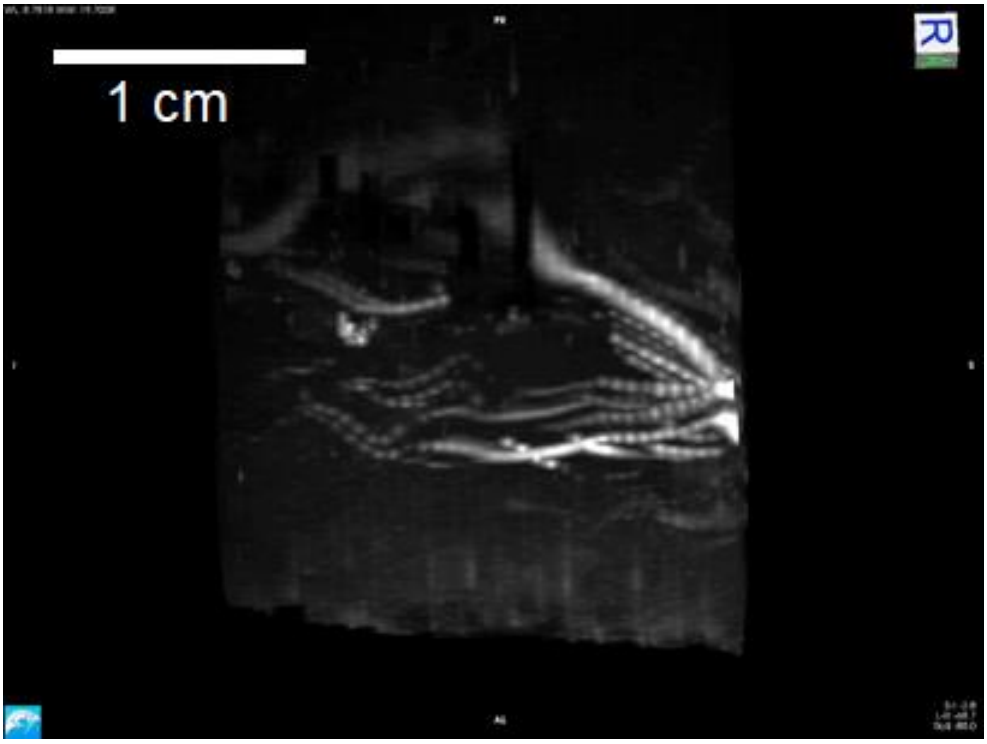

Figure 5-6 3D Angiography MIP sagittal plane.
It is showing the blood vessels in the fish head. The right side of the image is rostral, the left side caudal, the upper side dorsal and the lower side ventral. The bright structures are the blood vessels in the head of polar cod. The mouth cavity and the gills were removed digitally.

5.3 *In vivo* measurement of blood distribution of the brain of polar cod

5.3.1 Method Application

For the *in vivo* investigation of effects of elevated pCO_2 on the blood distribution to the fish's brain a set of MRI scanning protocols were developed and tested. The methods chosen for the in vivo trials were T_1-weighted FLASH scans, BOLD and phase contrast imaging.

5.3.1.1 Phase Contrast MRI

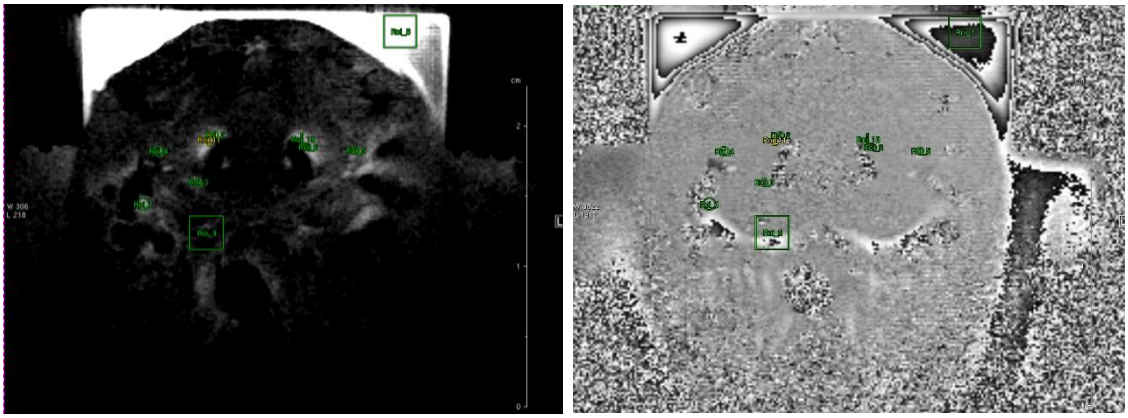

Figure 5-7 example axial phase contrast imaging scans.
On the left a phase contrast angiography reconstruction and a velocity map reconstruction on the right. Marked in green and yellow are the respective ROIs. The images show the cross-section of the fish. In the left images flow is displayed as bright. The bright areas on top represent water flowing around the fish and the bright areas within the fish represent blood and water in the mouth cavity in the fish. The right image is a velocity map reconstruction of the same scan representing flow velocity and direction by brightness.

Strong aliasing was observed in the top left and top right corner of the images were water was flowing with velocities far beyond the set flow speed in all *in vivo* scans. These aliasing effects were not observed within the fish.

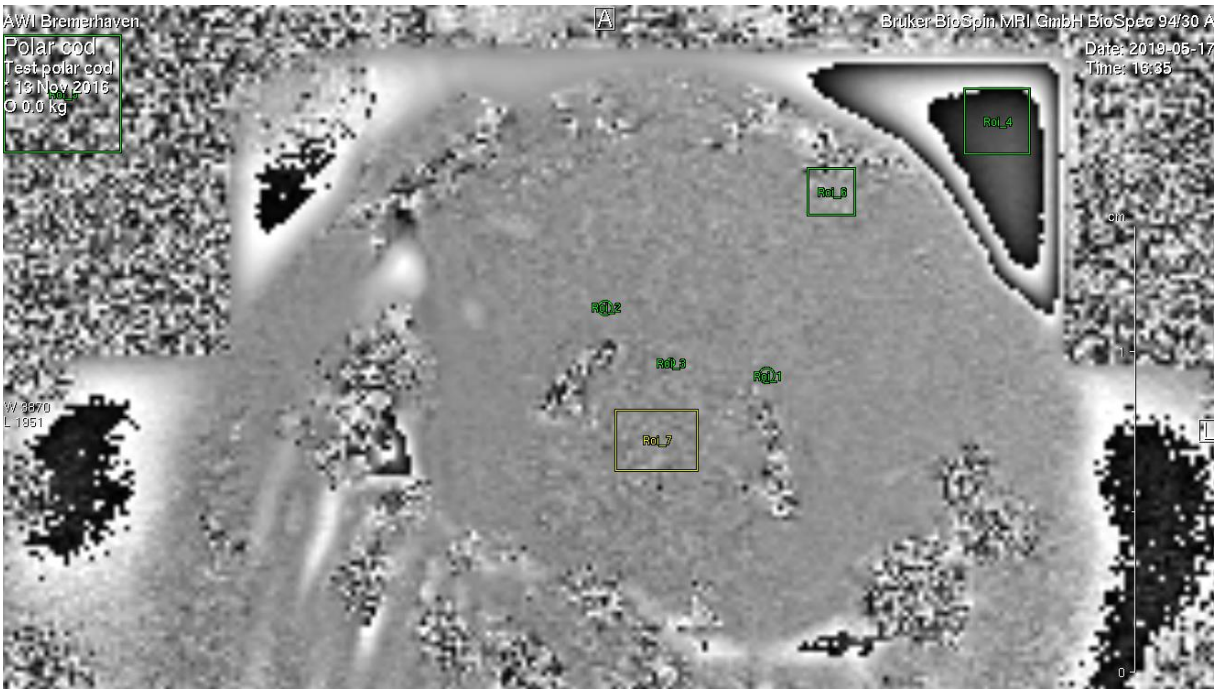

Figure 5-8 Axial phase contrast imaging scan of fish 6 with ROIs annotated in their respective position.

In fish 6 changes in blood flow could be observed in ROI 1 to ROI 3 comparing control and treatment conditions (see time series plot in Figure 5-9). The ROIs 1 and two were placed laterally over the blood vessels on top of otolith organs. The third ROI was placed over the vessel that lies centrally between them.

The mean blood flow per scan seemed to be relatively stable over the whole trial showing small fluctuations that did not obviously coincide with the treatment. Due to movement of the fish only one phase contrast image could be evaluated for the pre-treatment control of the fish. This scan was compared to 6 scans under treatment conditions before the fish moved again and ROIs had to be re-adjusted.

In ROI 1 the mean blood flow in the first scan before treatment was 0.569 cm/s (standard deviation 0.257) and in the second scan mean blood flow was 0.462 cm/s (standard deviation 0.225). The first scans under treatment conditions showed a flow of 0.149 cm/s (standard deviation 1.470). After that blood flow increased again with 0.253 cm/s (standard deviation 0.673) in the last scan before the fish moved and ROIs had to be adjusted. For the ROIs 2 and 3 the mean blood flow was lower for the first six scans under treatment conditions than in the compared scans under control conditions. For ROI 2 the mean blood flow before treatment was 0.42 cm/s (standard

deviation 0.098) compared to 0.285 cm/s (standard deviation 0.066) under treatment conditions. For ROI 3 the mean blood flow before treatment conditions was 0.298 cm/s (standard deviation 0.0.074) compared to 0.234 cm/s (standard deviation 0.140) under treatment. To conclude, in all three ROIs the blood flow decreased during the first 1.5 h of treatment conditions compared to the pre-treatment control. In ROI 1 and 2 the blood flow decreased gradually until it reached a minimum at 1 hour after beginning of the treatment and recovered again. For ROI 3 which covered the central vessel no obvious trend was detectable although the mean blood flow also was decreased during the first 1.5 h of treatment

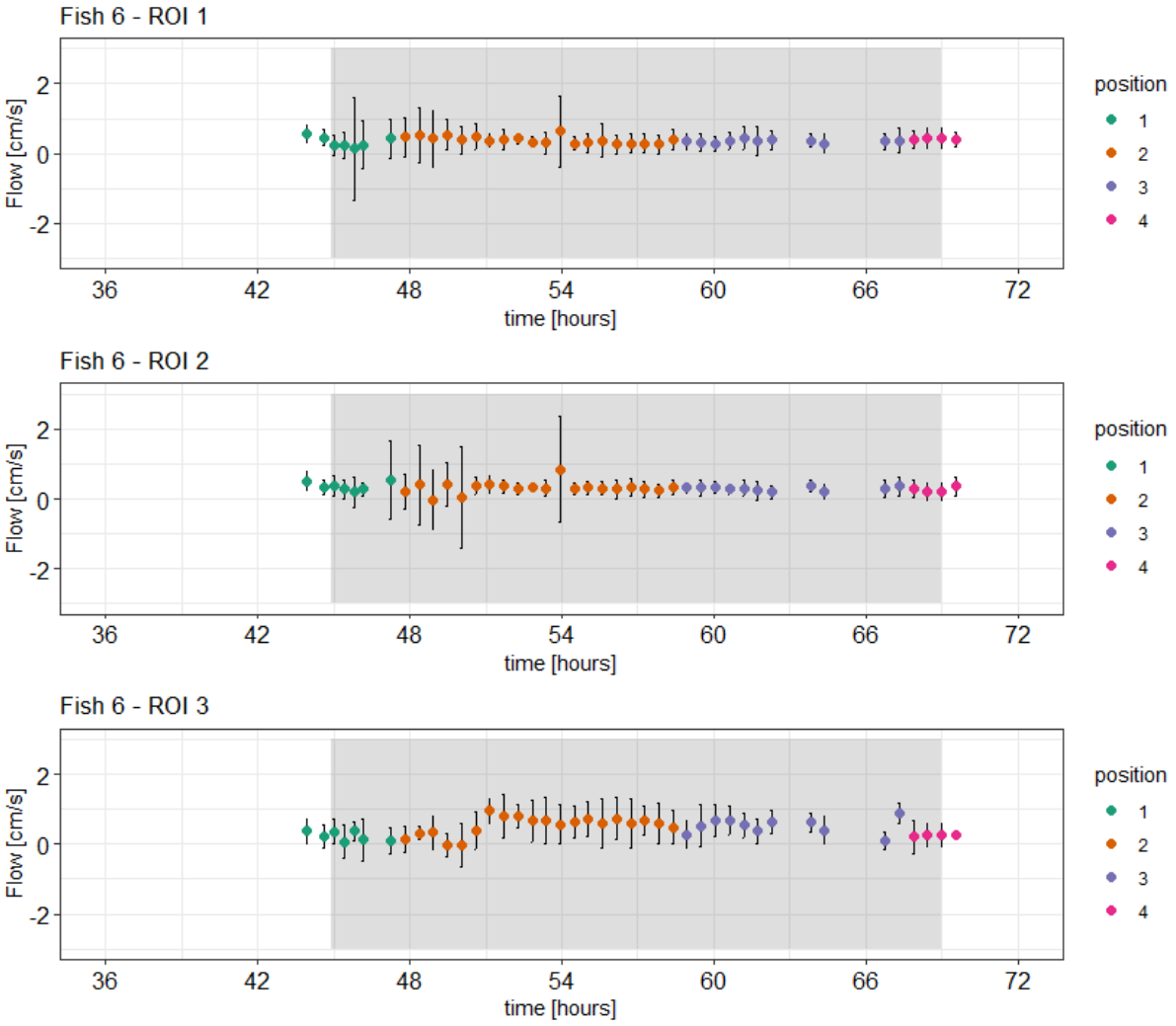

Figure 5-9 Time series of measured blood flow in ROI 1, ROI 2 and ROI 3 in fish 6.
Blood flow was compared for both treatments. The grey areas show the measurement under treatment conditions while the areas with white background show measurements at normocapnic control conditions. The x-axis shows time in hours and the y-axis represents mean blood flow in cm/s the respective ROI with error bars indicating the respective standard deviation. The dots are coloured according to the position of the respective ROI. As it moved at certain occasions over the trial the ROIs had to be adapted accordingly. The time axis starts at zero hours after the end of the acclimation phase when handling stress could be excluded.

For fish 7 the same analysis was conducted. Due to repeated movement of the animal over the course of the trial the ROIs had to be rearranged repeatedly to exclude motion artefacts. This led to a division of 7 position for each respective ROI in fish 7 (see time series in Figure 5-10). The ROIs 1, 2, 3, 4, 5, 6 had the shape of circles and were placed over identified as blood vessels in PCA scans. The ROIs 7, 8, 9 and 10 were of rectangular shape and placed to concern for noise and aliasing. Therefore, they were positioned in the area of the image that represents water in the chamber, air around the chamber and tissue of the animal.

The mean blood flow in ROI 1 ranged from 0.040 to 1.61 cm/s with a median of 0.482 cm/s. Before treatment the median in ROI 1 was 0.711 cm/s. After the treatment was administered, the blood flow increased up to 1.61 one hour after treatment began

Due to software failure while measuring fish 7 nearly 6 hours of treatment could not be supervised by scans or spectra. Also, in fish 7 unfortunately no blood flow data could be obtained from phase contrast images for the after-treatment control due to strong motion artefacts as the fish was moving repeatedly in this phase. Therefore, the evaluation of possible after-effects could not be performed.

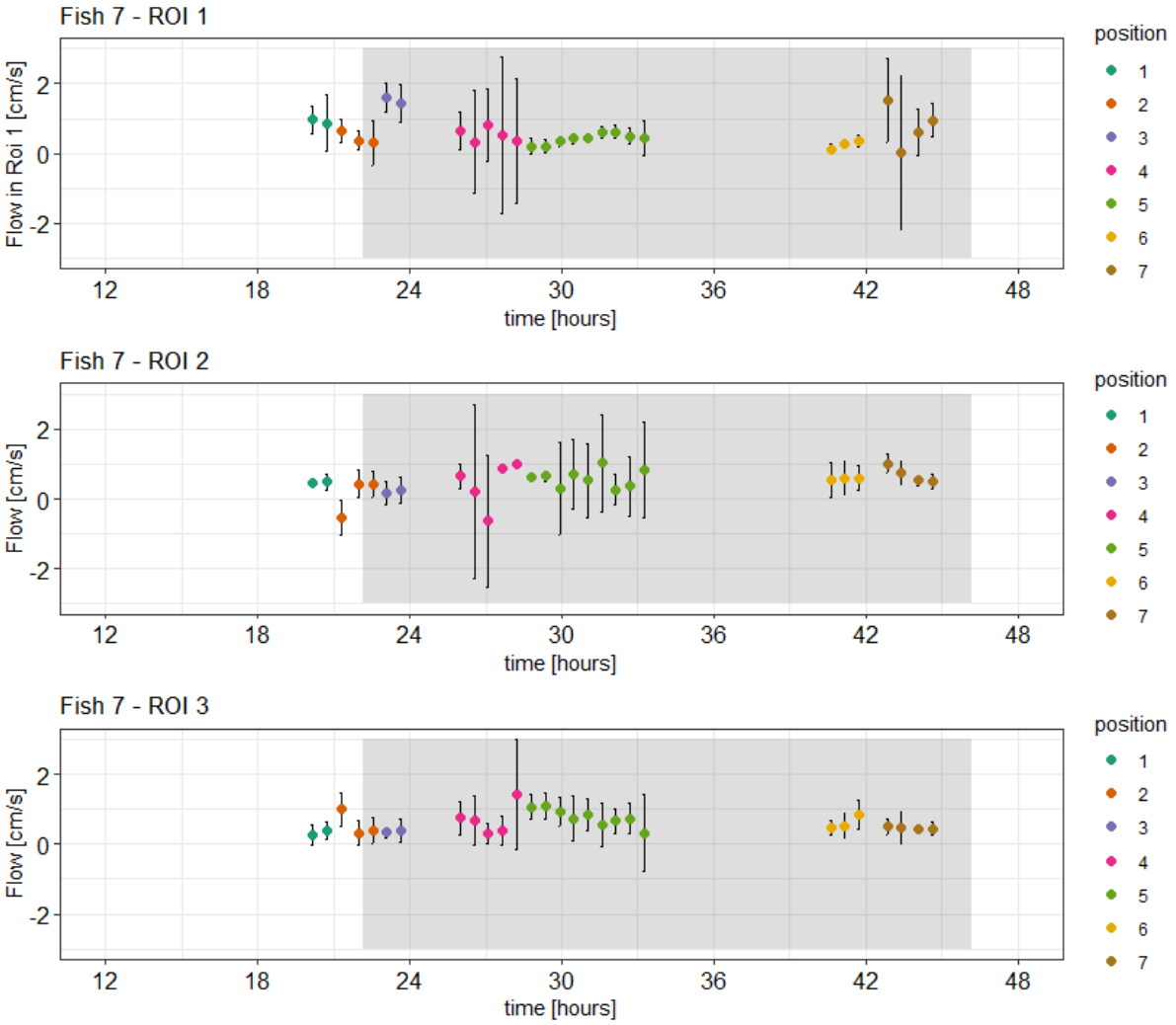

Figure 5-10 Time series of measured blood flow in ROI 1, ROI 2 and ROI 3 in fish 7.
The blood flow was compared for both treatments. The grey areas show the measurement under treatment conditions while the areas with white background show measurements at normocapnic control conditions. The x-axis shows time in hours and the y-axis represents mean blood flow in cm/s the respective ROI with error bars indicating the respective standard deviation. The dots are coloured according to the position of the respective ROI. As it moved at certain occasions over the trial the ROIs had to be adapted accordingly. The time axis starts at zero hours after the end of the acclimation phase when handling stress could be excluded.

For the ROIs 4, 6 and 6 which were placed on structures believed to be peripheral blood vessels no effect could be observed. Due to the frequent repositioning of ROIs and the relatively high standard deviations of the measurements in these ROIs the data is inconclusive (see Figure 5-11).

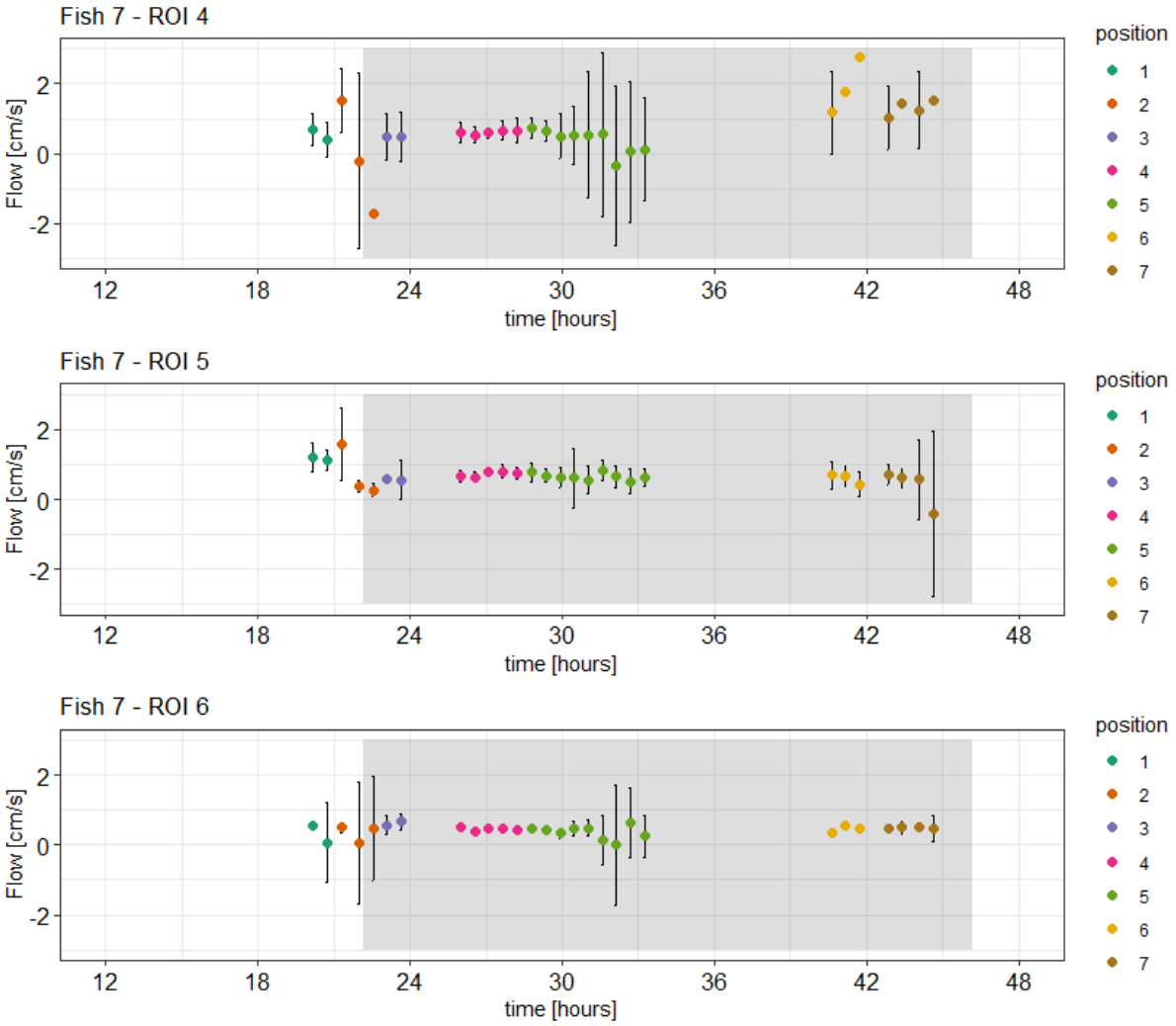

Figure 5-11 Time series of measured blood flow from phase contrast imaging in ROI 4, ROI 5 and ROI 6 in fish 7.
Blood flow was compared for both treatments. The grey areas show the measurement under treatment conditions while the areas with white background show measurements at normocapnic control conditions. The x-axis shows time in hours and the y-axis represents mean blood flow in cm/s the respective ROI with error bars indicating the respective standard deviation. The dots are coloured according to the position of the respective ROI. As it moved at certain occasions over the trial the ROIs had to be adapted accordingly. The time axis starts at zero hours after the end of the acclimation phase when handling stress could be excluded.

5.3.1.2 Slow Blood Flow Imaging

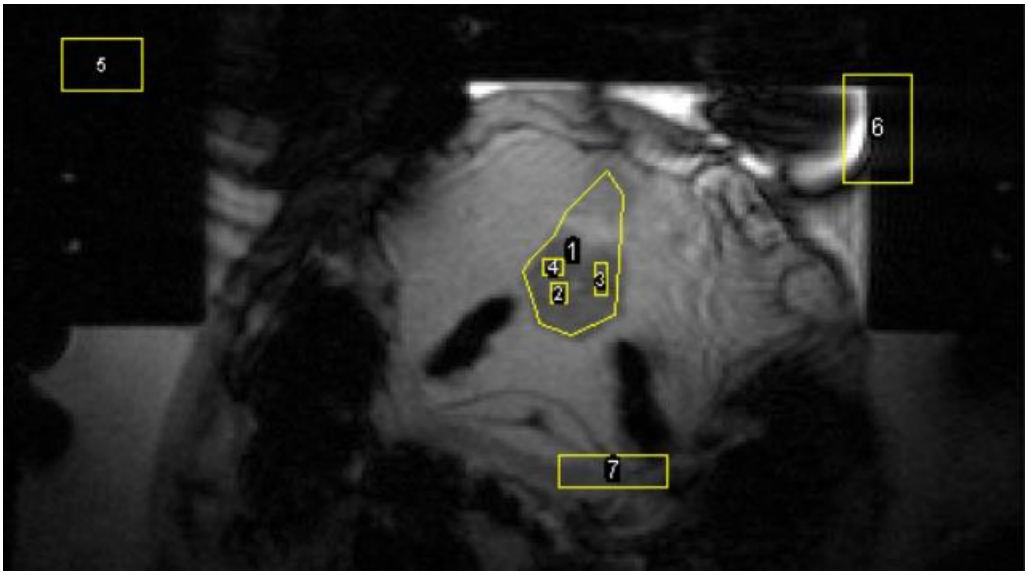

Figure 5-12 FLASH axial MRI image annotated with ROIs of Polar cod (fish 6) in vivo

In fish 6 seven ROIs were defined. Four of these ROIs were set over the fish brain and three were defined to serve as reference in tissue, air and water to identify possible artefacts. ROI 1 was a polygon covering the whole cross-section of the brain. ROI 2, 3 and 4 were rectangles spread over the brain's cross-section. Due to movement of the fish positions of the ROIs had to be rearranged three times for fish 6. In ROI 1 there appeared to be slight decrease in signal intensity. In ROI 2 there were no obvious alterations. Over the first 5 hours of treatment there appeared to be an increase in signal intensity in the ROIs 3 and 4 (see Figure 5-13). There were no considerable differences between post-treatment control and treatment conditions.

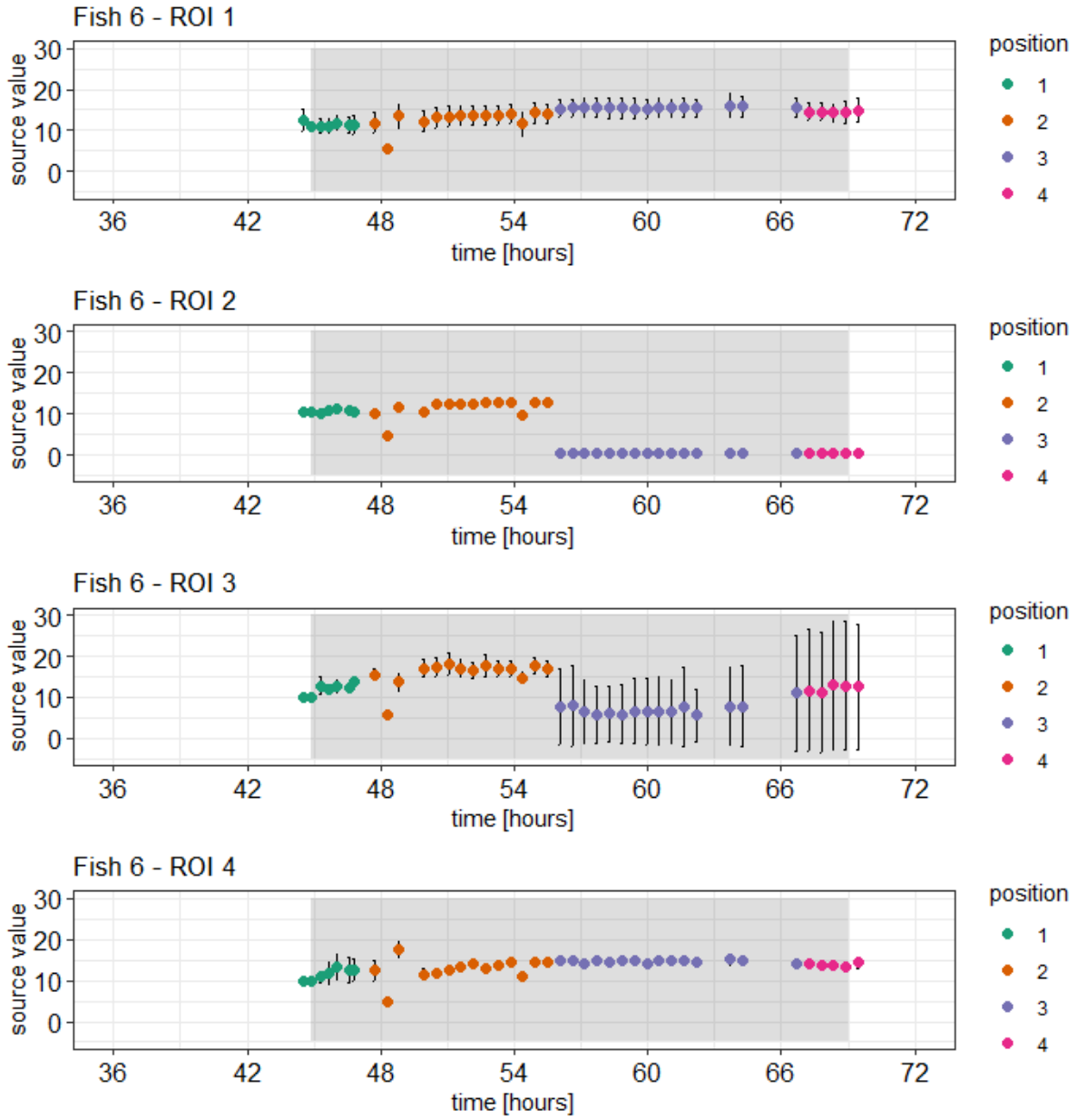

Figure 5-13 Time series of signal intensity from T_1-weigthed imaging in ROI 1-4 in fish 6.
Signal intensity was compared for both treatments. The grey areas show the measurement under treatment conditions while the areas with white background show measurements at normocapnic control conditions. The x-axis shows time in hours and the y-axis represents mean blood flow in cm/s the respective ROI with error bars indicating the respective standard deviation. The dots are coloured according to the position of the respective ROI. As it moved at certain occasions over the trial the ROIs had to be adapted accordingly. The time axis starts at zero hours after the end of the acclimation phase when handling stress could be excluded.

In fish 7 the position of the ROIs had to be rearranged 6 times. Position 2 of the ROIs covers the transition from control to treatment with one scan before and on under treatment. In ROI 1-4 no considerable difference in signal intensity could be observed for those scans. Even though, the fish moved, and ROIs had to rearranged, it appears

that blood flow differed between one and 5 hours after the treatment was started. In ROI 1 the signal intensity increased after 1.5 h and appeared to be normalized after 4 hours.

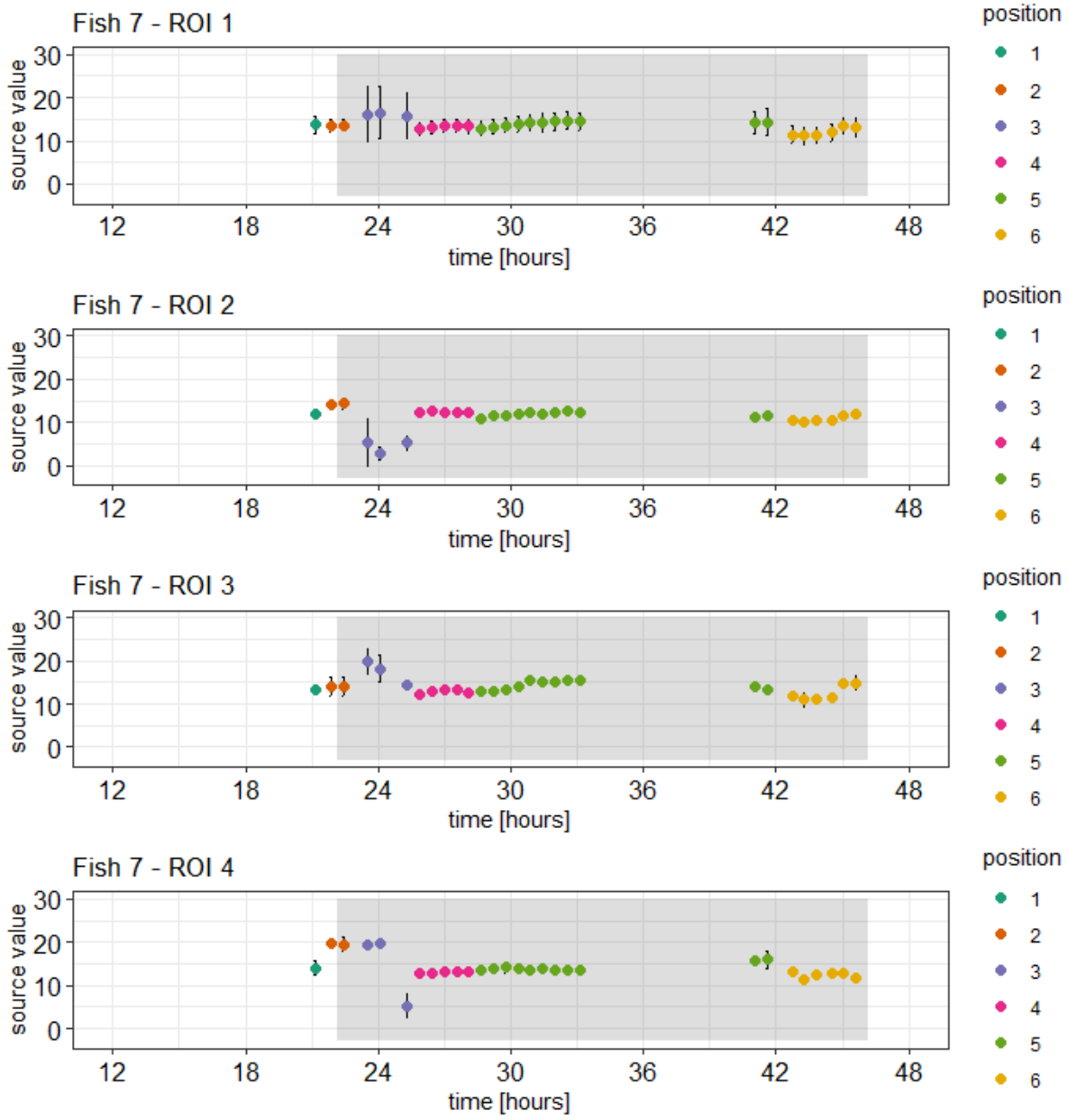

Figure 5-14 Time series of measured signal from T_1-weigthed imaging intensity in ROI 1-4 in fish 7. Signal intensity was compared for both treatments. The grey areas show the measurement under treatment conditions while the areas with white background show measurements at normocapnic control conditions. The x-axis shows time in hours and the y-axis represents mean blood flow in cm/s the respective ROI with error bars indicating the respective standard deviation. The dots are coloured according to the position of the respective ROI. As it moved at certain occasions over the trial the ROIs had to be adapted accordingly. The time axis starts at zero hours after the end of the acclimation phase when handling stress could be excluded.

5.3.1.3 BOLD Imaging

To investigate possible changes in brain perfusion under ocean acidification BOLD MRI measurements were performed. ROIs were used too analyses of the signal intensities of the images. ROIs were adjusted in size and position if the fish moved. Up to two ROIs were positioned to cover the brain in total with a polygon fitting to its size and three rectangles placed in the ventral, dorsal and on side of the brain to accord for possible effects due to gradients and signal intensity loss due to distance from the surface coil. Additional rectangular ROIs were placed in areas of the image that represented water in the chamber, air outside the chamber and body tissue.

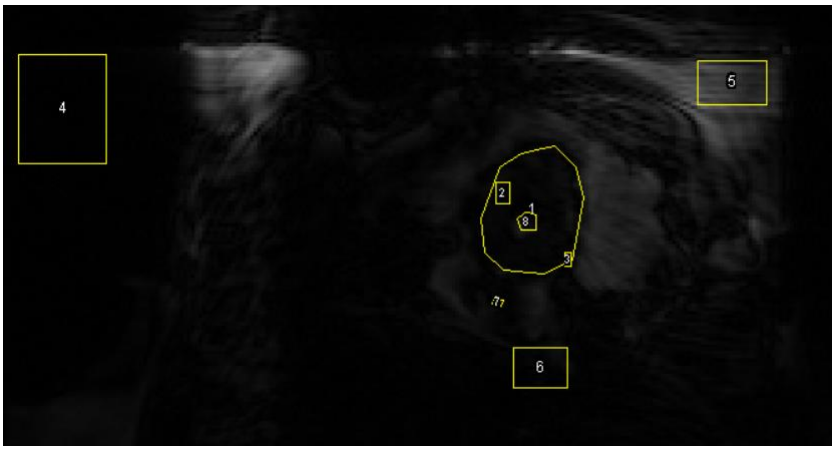

Figure 5-15 BOLD axial MRI image annotated with ROIs of Polar cod (fish 6) in vivo.

In fish 6 four ROIs (ROI 1, ROI 2, ROI 3, ROI 4) were placed over the fish's brain in axial BOLD imaging to investigate perfusion changes under treatment conditions compared to control conditions. The ROI 1 was fitted to cover the whole cross-section of the brain while ROI 2 and 3 only covered parts of it. ROI 1 was designed to be a polygon covering as much of the brain cross-sections area as possible. ROI 2 and 3 where rectangles only covering a small portion of the brain and were placed in different positions (see Figure 5-15). This should account for possible spatial differences and allow a comparison between the whole cross-section and parts of it. Additional ROIs were placed in the periphery in body tissue, flowing water and air outside the chamber to be able to account for possible artefacts. Due to movement of the fish during control and treatment phase some images could not be evaluated due to motion artefacts. As some of these movements led to a slight change in position of the fish the ROIs had to

be adapted to continue covering the respective area. Therefore, six ROI positions had been identified after respective movements.

The first continuous analysis of ROI in fish 6 start at 55 minutes after beginning of the treatment so no control values could be obtained. This position could be analysed for approximately 1.5 hours before the fish started to move again. During these phase the measured signal intensities in the ROI 1 did vary slightly but no trend was observable. In ROI 2 a strong increase in signal intensity was measured till circa 2h after treatment began. After this peak, a decline seemed to start. In ROI 3 the contrary could be observed as the values decreased. ROI 4 was placed to be outside the chamber. It showed values slightly above zero, which was expected, for all positions except position 2.

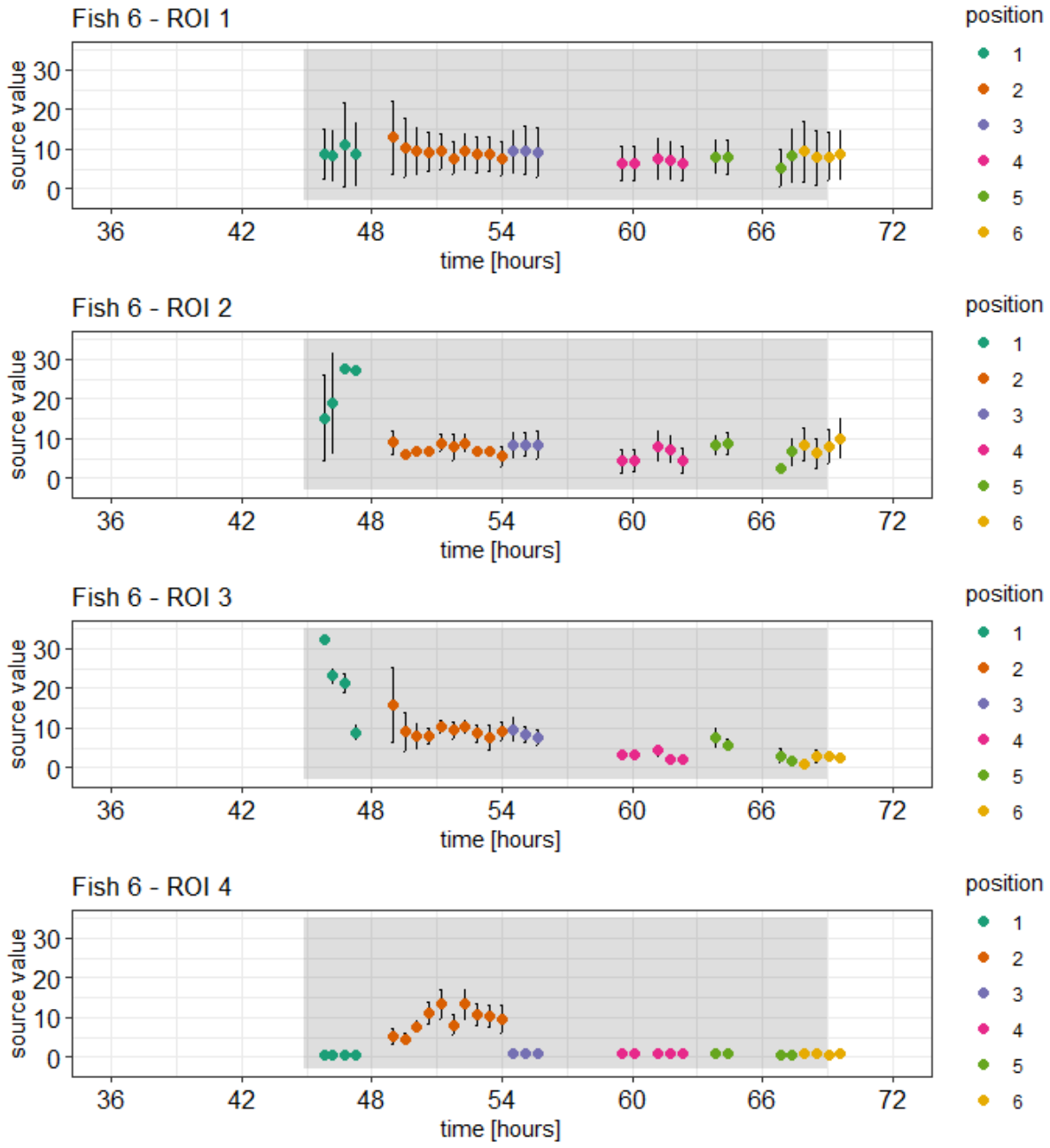

Figure 5-16 Time series - BOLD in vivo MRI scans of fish 6 in ROI 1- 4 in fish 7.
Signal intensity was compared for both treatments. The grey areas show the measurement under treatment conditions while the areas with white background show measurements at normocapnic control conditions. The x-axis shows time in hours and the y-axis represents mean signal intensities the respective ROI with error bars indicating the respective standard deviation. The dots are coloured according to the position of the respective ROI. As it moved at certain occasions over the trial the ROIs had to be adapted accordingly. The time axis starts at zero hours after the end of the acclimation phase when handling stress could be excluded.

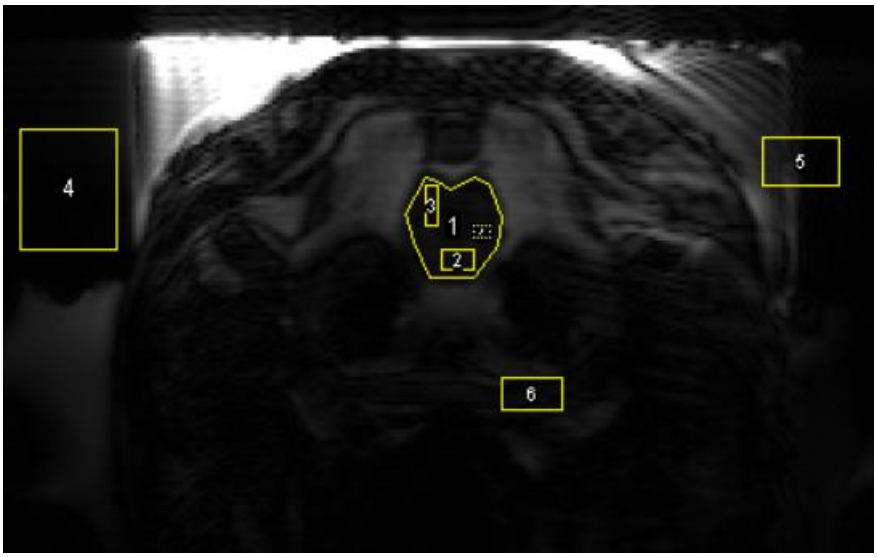

Figure 5-17 BOLD axial MRI image annotated with ROIs of Polar cod (fish 7) in vivo.

Due to movement the position of the ROIs had to be rearranged 6 times and 17 scans could not be evaluated due to movement artefacts. Again 6 ROIs were placed over the images, with ROI 1 as polygon covering the cross-section of the brain, ROI 2 and 3 as rectangles spread over the cross-section of the brain and ROI 4-6 as references. After 1 hour of treatment there appeared to be an increase in signal intensity in ROI 1 and 2 and an slight decrease in ROI 3. After 4 hours there is another increase in signal intensity in ROI 1 and 2 leading to a peak at 9 hours after the begin of treatment and then reducing again. Even though, the increase in signal intensity appears way stronger in ROI 1, nearly doubling from 6.7 to 12.9, than in 2 the temporal pattern was similar. The standard deviation in ROI 1 was also comparably higher than in ROI 2 (see Figure 5-18).

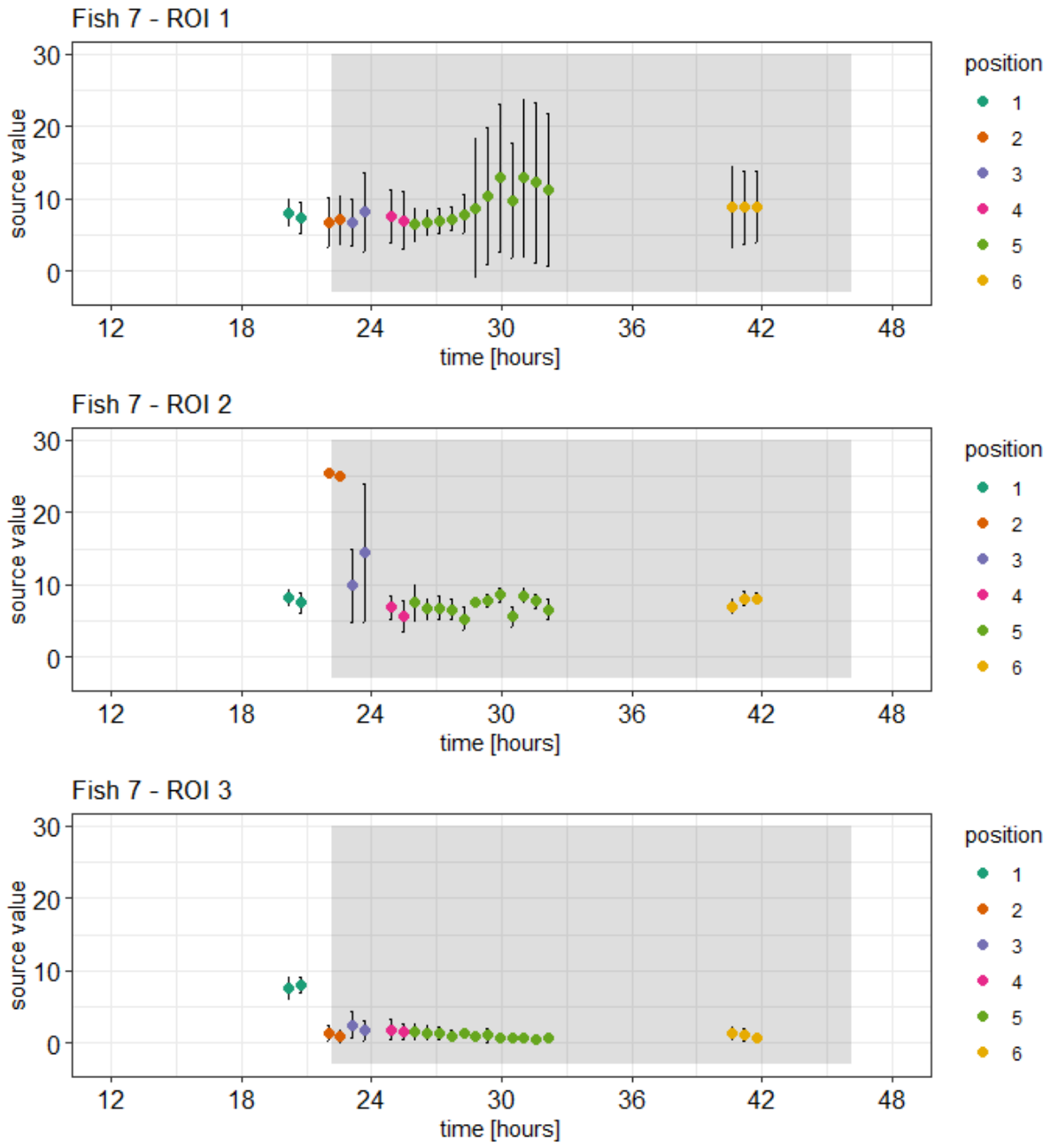

Figure 5-18 Time series - BOLD in vivo MRI scans of fish 7 in ROI 1-3 in fish 7.
Signal intensity was compared for both treatments. The grey areas show the measurement under treatment conditions while the areas with white background show measurements at normocapnic control conditions. The x-axis shows time in hours and the y-axis represents mean signal intensities the respective ROI with error bars indicating the respective standard deviation. The dots are coloured according to the position of the respective ROI. As it moved at certain occasions over the trial the ROIs had to be adapted accordingly. The time axis starts at zero hours after the end of the acclimation phase when handling stress could be excluded.

5.4 *In vivo* measurement of intracellular pH and the energy metabolism of the brain of polar cod

5.4.1 Indices for the cellular energetic state *in vivo*.

In trials in fish 6 the mean P_i-PCr-ratio in the control before treatment was 0.102 (standard deviation of 0.030). The mean P_i-PCr-ratio during treatment was 0.096 (standard deviation of 0.028). The P_i-PCr-ratio was 0.006 lower under treatment condition. In the time series plot (Figure 5-21) a relatively strong decrease in P_i-PCr-ratio happened in the first 3 hours of treatment and is followed by a recovery until approximately 6 hours after beginning of the treatment.

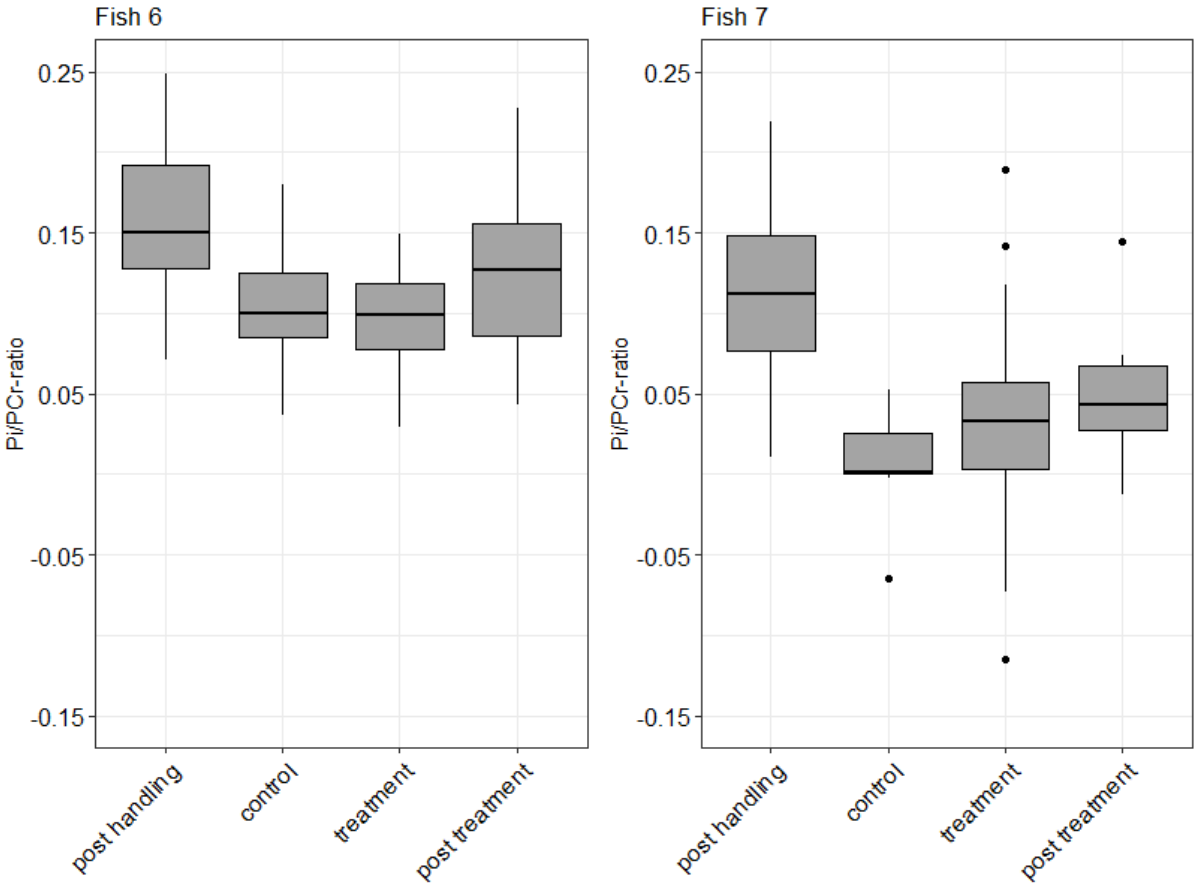

Figure 5-19 Boxplots showing the P_i-PCr-ratio for fish 6 and fish 7 compared by experimental category (post handling, control, treatment, post treatment).

The mean signal intensity of βATP in the pre-treatment control was 0.001 (standard deviation of 0.285). Under treatment conditions the mean signal intensity of βATP was -0.057 (standard deviation of 0.269). The mean under treatment conditions was 0.058

lower compared to the pre-treatment control. The temporal pattern of decrease and recovery is very similar to the pattern described in the P_i-PCr-ratio although the fluctuations around the mean appear to be stronger and the signal intensity of βATP appears to decrease during the last three hours of treatment.

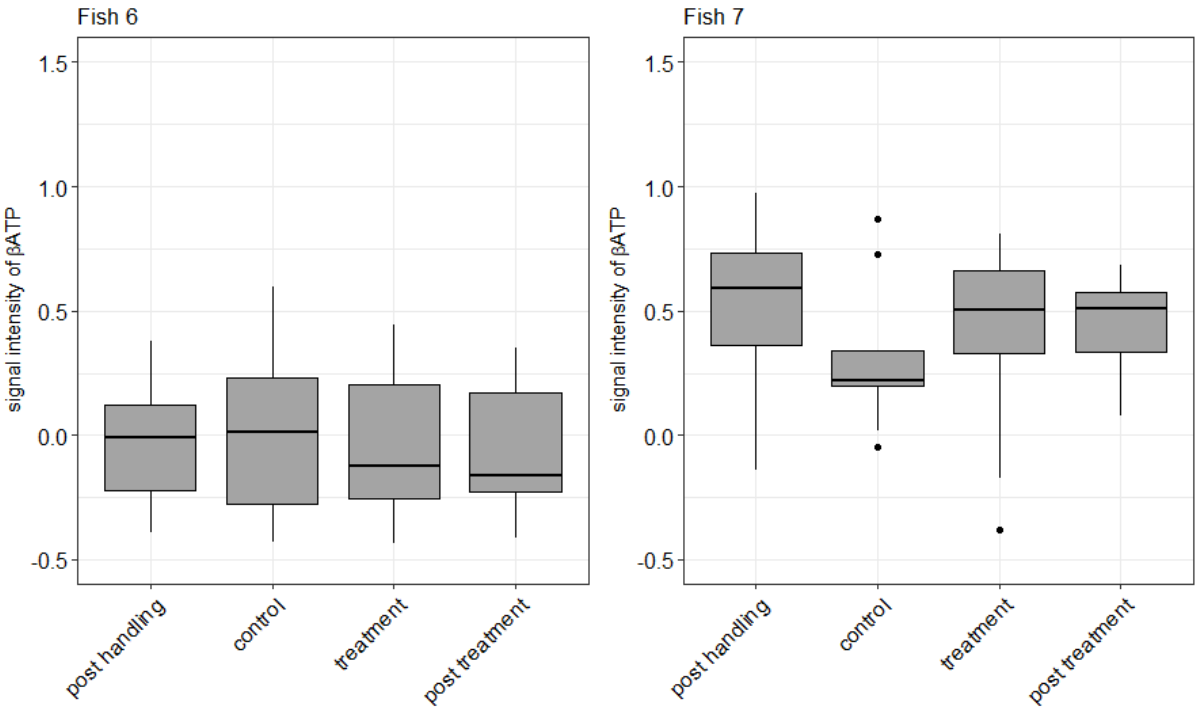

Figure 5-20 Boxplots showing the βATP signal intensity for Fish 6 and Fish 7 compared by category (post handling, control, treatment, post treatment).

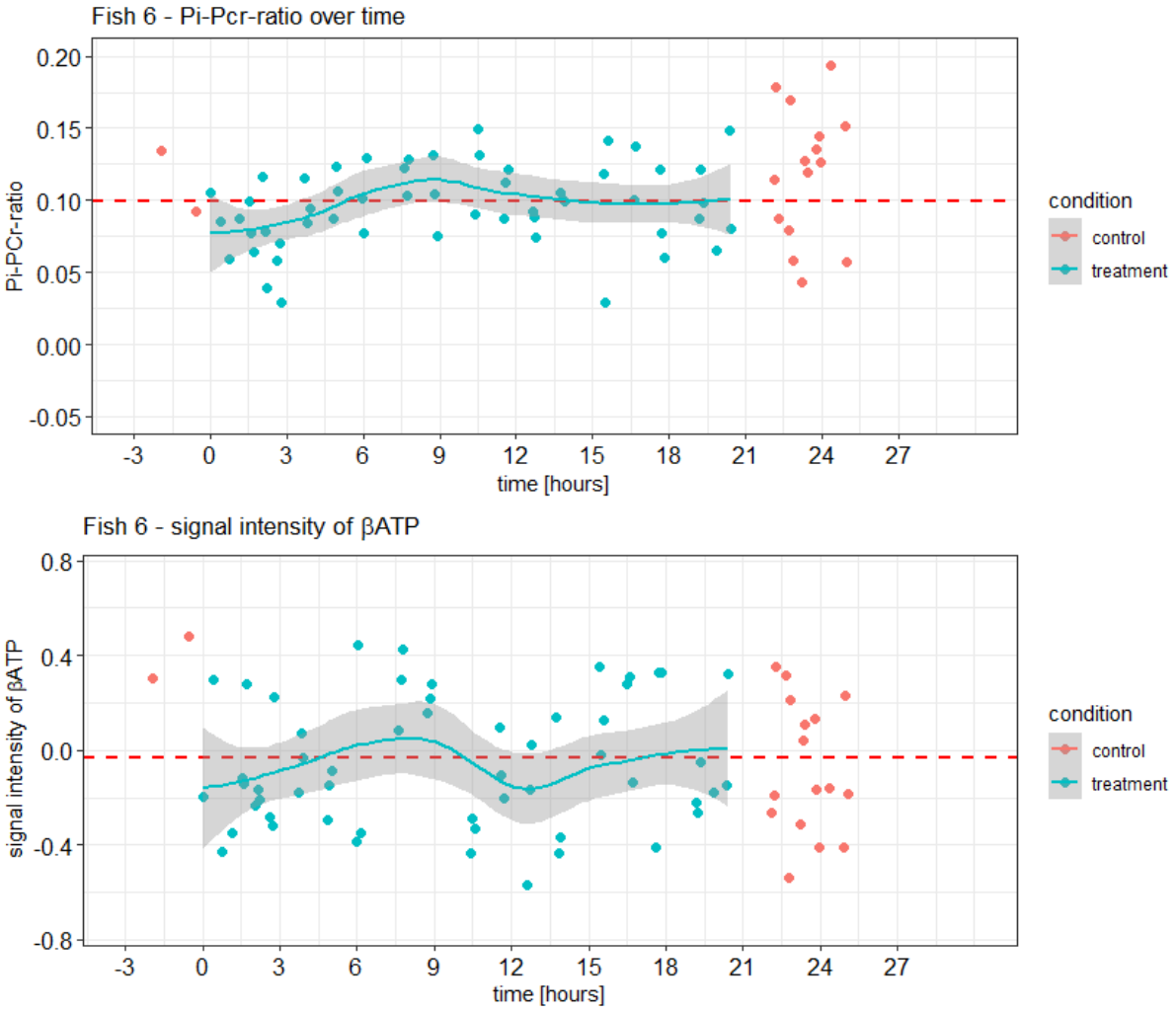

Figure 5-21 Time series plots of the P_i-PCr-ratio (top) and βATP signal intensity in fish 6 over time. The control phase is blotted in red and the respective treatment phase in blue. The red dotted line shows the mean of the pre-treatment control. The blue line plotted fit in both graphs follows the method loess with a local regression to the closest 0.7 points (Wickham 2016). The time 0 is the start of the treatment.

In fish 7, the mean P_i-PCr-ratio in the control before treatment beginning was 0.007 (standard deviation of 0.033). The mean P_i-PCr-ratio during treatment application was 0.034 (standard deviation of 0.046) which is an increase of 0.027. The mean signal intensity of βATP in the pre-treatment control was 0.317 (standard deviation of 0.302). During the treatment the mean signal intensity of βATP was 0.4383769 (standard deviation of 0.288). The mean signal intensity of βATP showed an increase of 0.121 during treatment conditions. The signal intensity during treatment conditions only lowered to levels of the pre-treatment mean after 8 hours of treatment and again during the last six hours of treatment. A similar impression is given by time series plot (Figure 5-22) for the P_i-PCr-ratio albeit the fluctuations seemed minor.

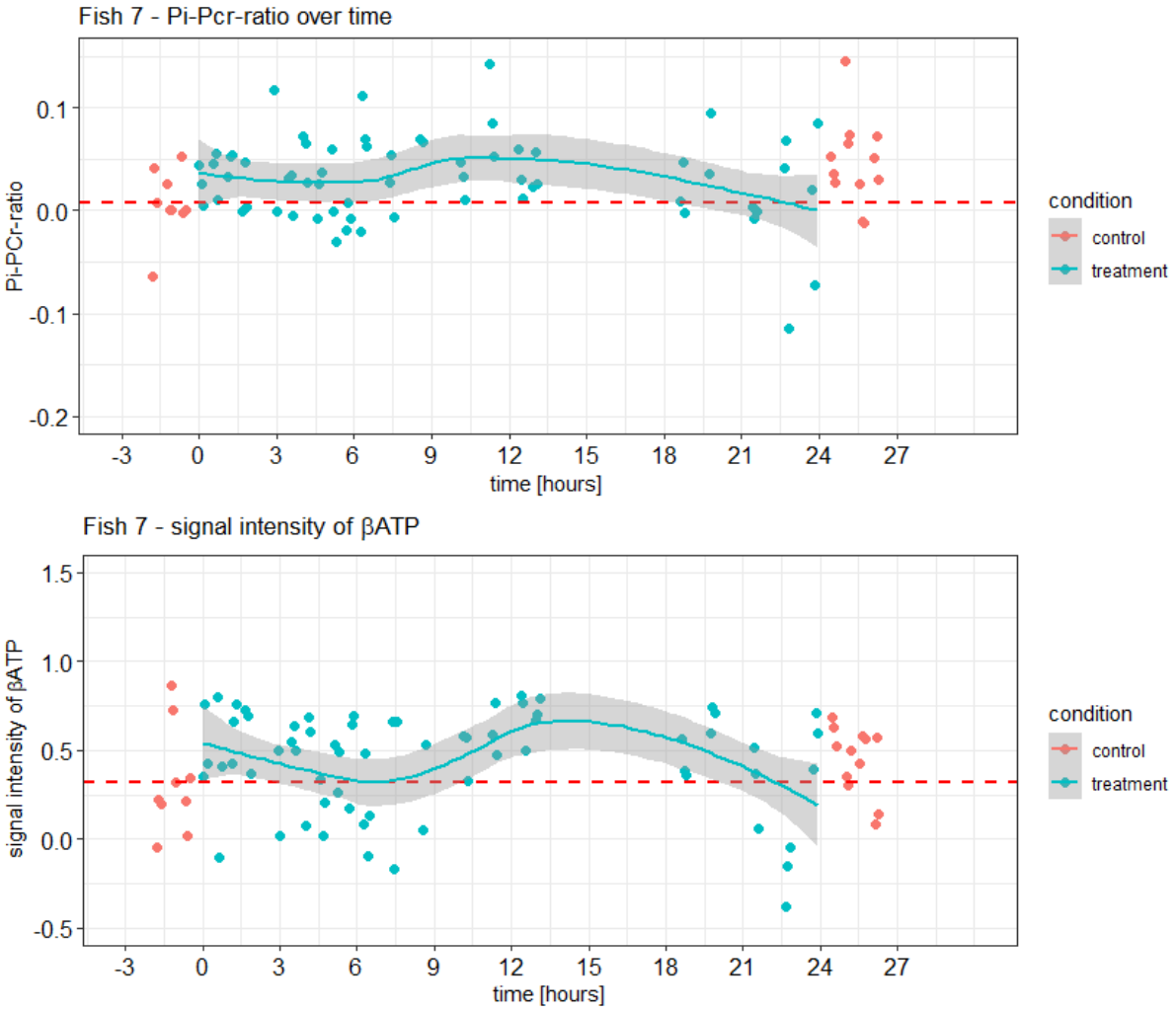

Figure 5-22 Time series plots of the PI/PCr-ratio (top) and βATP concentration in fish 7 time.
The control phase is blotted in red and the respective treatment phase in blue. The red dotted line shows the mean of the pre-treatment control. The blue line plotted fit in both graphs follows the method loess with a local regression to the closest 0.7 points (Wickham 2016). The time 0 is the start of the treatment.

5.4.2 *In vivo* measurement of intracellular pH and the energy metabolism of the brain of polar cod

Right, after the handling ended and the trials started measured chemical shift were down till 5.07 ppm in fish 6 and stabilized at around 5.5 ppm over the course of six to 18 hours (see Figure 5-24). After the handling the pH_i was as low as 7.11 and stabilized at 7.49.

In spectra obtained during and after acclimation the position of the peak of PCr did not vary. The pHi, calculated from chemical shift of Pi, on the other side did vary between acclimation and after it (Figure 5-23). During the first 18 hours after handling the mean pH_i was lower than after acclimation and did gradually increase to physiological levels (see Figure 5-24). Therefore, it was decided to evaluate control data after a 18-hour acclimation phase. The integral under the Pi peak, representing the concentration of Pi in the measured tissue, was substantially higher right after handling and did reduce gradually over the acclimation period (see chapter 5.4.1).

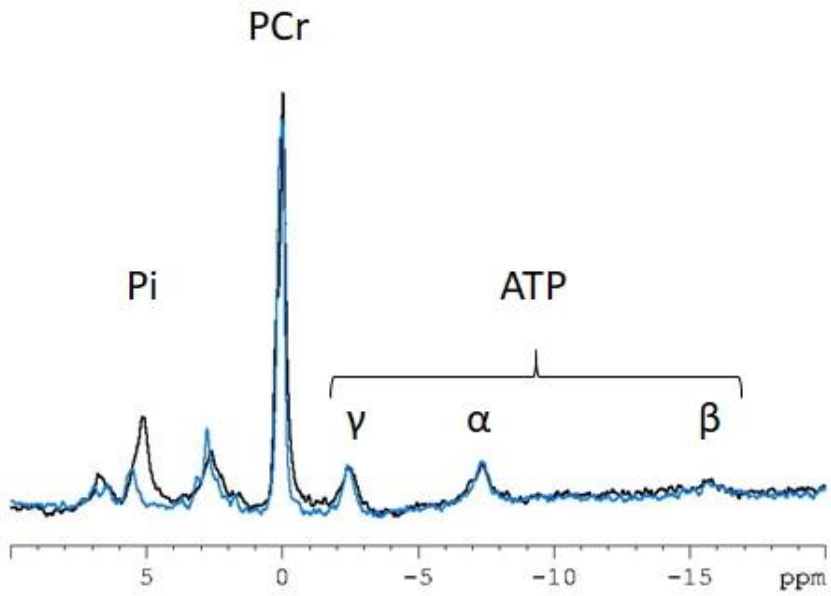

Figure 5-23 Comparison of sum spectra of a fish after handling and after 18h post handling.
Comparison of a sum spectrum of 3 consecutive spectra obtained during acclimation phase right after handling (black line) and a sum spectrum of 3 consecutive spectra obtained after acclimation (blue line) in fish 7 under normocapnic conditions. The spectra show a difference in peak size between acclimation and after acclimation of the Pi-signal and a difference in chemical shift of Pi indicating a difference in pHi.

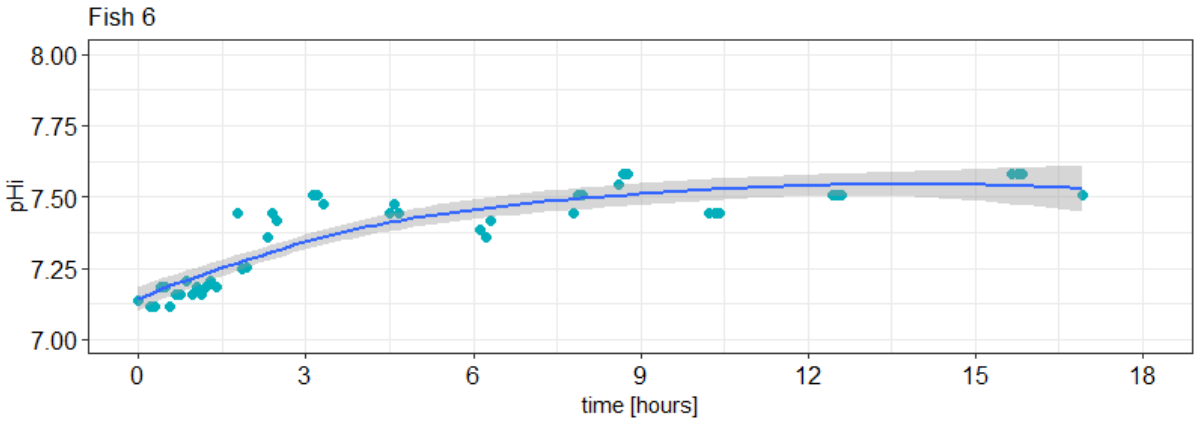

Figure 5-24 Time series of pHi from 31P NMR over the post-handling acclimation phase.
Spectra obtained in fish 6 over the acclimation phases of 18 hours. The x-axis shows the time in hours from start of the experimentation and the y-axis shows the pHi calculated from chemical shift. The plotted fit follows the method loess with a local regression to the closest 1.5 points (Wickham 2016).

Some spectra of fish 7 showed two peaks at range between 5.1 ppm to 5.8 ppm were the Pi signal was expected (see Figure 5-25). In this case the peak closer to the physiological chemical shift of 5.55 (corresponds to a pH of 7.5) was evaluated. The appearance of this second peak did not appear to be associated with movement of the fish and was detected in multiple blocks of consecutive spectra.

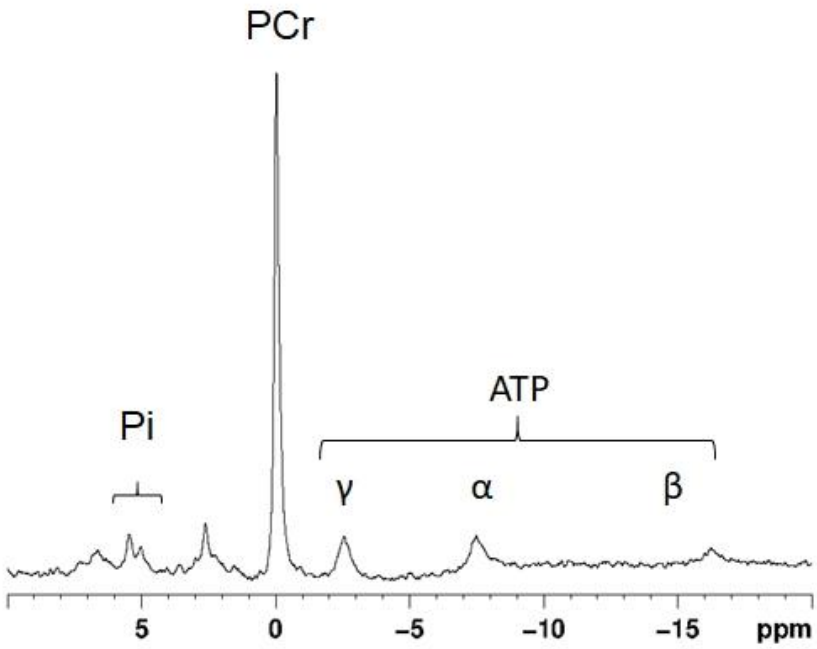

Figure 5-25 ^{31}P NMR sum spectrum showing a double peak around the δ of Pi.
Sum spectra of 3 consecutive spectra in fish 7 under normocapnic conditions showing two peaks at the position of Pi (at chemical shifts of 5.04 and 5.46 representing pH values of 7.1 and 7.45 respectively).

In Fish 6 a mean pre-treatment control pH_i of 7.59 (standard deviation of 0.14) was calculated from the measured chemical shifts. A mean pH_i of 7.53 (standard deviation of 0.116) during treatment conditions was calculated for the same fish. The pH_i decreased about 0.057. under treatment conditions (see Figure 5-26). In Fish 7 the derived pH_i was 7.594 (standard deviation of 0.138) under control conditions before the treatment. The mean pH_i under treatment conditions was 7.585 (standard deviation of 0.133). The pH_i decreased marginally about 0.009 under treatment conditions. In Fish 6 pH_i under control conditions after treatment was 7.569 (standard deviation of 0.091). For fish 7 the mean pH_i under control conditions after the treatment was 7.58 (standard deviation of 0.046).

When comparing the mean pH_i over the whole control time with the mean pH_i over the whole treatment phase of 24 h very subtle differences can be identified. The pH_i under treatment conditions is slightly lower than before treatment under control conditions for both fish. After treatment the pH_i increases slightly in fish 6 (see Figure 5-26). This increase could not be observed in fish 7.

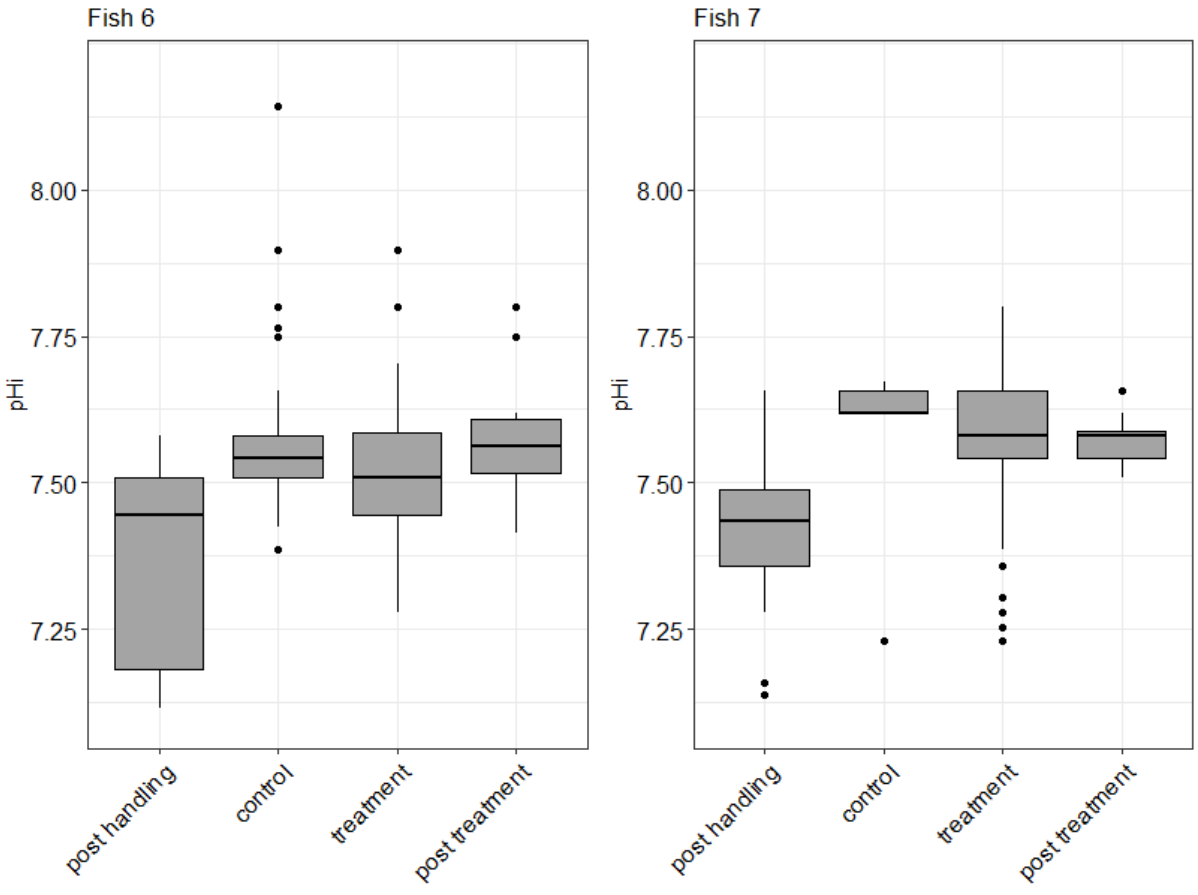

Figure 5-26 Boxplots showing the intracellular pH (pH_i), calculated from chemical shift, for fish 6 and fish 7 compared by experimental category (post handling, control, treatment, post treatment).

When comparing the distribution of pH_i values over the time of the treatment in fish 6 a slight but notable decrease in pH_i is visible after the treatment started. The reduction of pH_i has its minimum 3h 40min after the begin of the treatment at a pH_i of 7.39 and is followed by a gradual recovery to values close to the pre-treatment control mean of pH_i 7.587 (standard deviation of 0.141) with a mean pH_i of 7.53 (standard deviation of 0.115) during treatment (see Figure 5-27). For fish 7 the data does not provide a clear trend but apparently the pH_i stayed relatively stable around the pre-treatment mean for around 8 hours of treatment before decreasing slightly, staying slightly below the mean of the pre-treatment control and recovering at the end of the treatment phase.

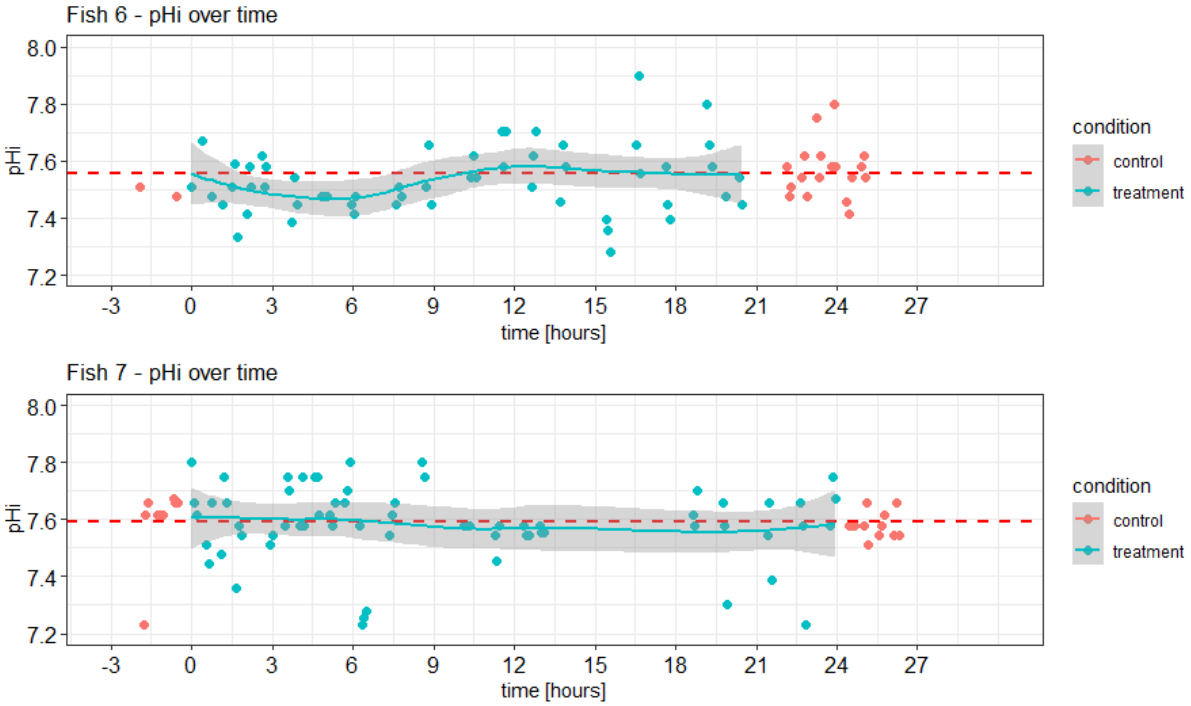

Figure 5-27 Time series of the pH_i by condition.
Measurements were conducted under pre-treatment control, treatment and post-control condition in fish 6 and 7. The upper graph shows the pH_i of fish 6 and the lower graph the pH_i of fish 7. All pH_i-values were calculated from chemical shifts measured using *in vivo* ^{31}P-NMR spectroscopy. The time series is truncated by the 18h acclimation phase. The plotted fit in both graphs follows the method loess with a local regression to the closest 0.7 points (Wickham 2016).

6 Discussion

6.1 Method Development and Evaluation

The main aim of this work was to adapt a set of non-invasive methods to investigate possible physiological effects of ocean acidification in the brain of polar cod. A multi-parameter protocol should be delivered to assess blood supply and alterations in the brain's energy metabolism and acid-base status. Therefore, an *in vivo* ^{31}P-NMR spectroscopy was applied in combination with different MR imaging techniques. Potential OA induced alterations in the blood supply of the brain, *In vivo* measurement of intracellular pH and the energy metabolism of the brain of polar cod, followed by changes in the energy and acid base status of the brain should have been investigated.

To evaluate the pH_i under normocapnic conditions and the effects of elevated pCO_2 a protocol (see 4.4.1) was followed to exclude handling stress. The handling- induced alterations in the brain's acid-base and energy status differed between individuals and depended on the needed handling time and effort to position the animal properly. A post handling resting phase of 18 hours was shown to be adequate to exclude handling associated effects on the energy status of the brain cells, the pH_i or the blood distribution and allowed stable and comparable physiological conditions. This finding supports the protocol used by Wermter *et al.* (2018). Over the curse of this study an array of imaging techniques was tested, and suitable ones have been chosen.

Rapid Acquisition with Relaxation Enhancement (RARE) MRI as well as Fast Low Angle Shot (FLASH) MRI scans were tried and compared for morphological imaging. As they did not differ substantially in features like acquisition time both methods were suitable for in vivo investigations of the brain morphology. Albeit, their general suitability it showed that their applicability was limited to certain tasks. The RARE imaging provided relatively high image contrasts and allowed discrimination between brain regions and surrounding tissues and even between different structures within brain areas. The RARE imaging did not allow the detection of blood flow or blood vessels. Whereas the FLASH imaging did not provide high contrast and was not very suitable for the discrimination of brain areas and tissues but did exhibit very strong signals even for small blood flows. Hence, it was suitable to detect blood vessels in the

head of the fish and explore the heads vascularity. Therefore, FLASH scans were used in the experiments to identify suitable blood vessels for the blood flow investigations.

^{31}P-NMR spectroscopy trials were conducted over control and treatment periods in fish 6 and 7 and compared. The mean pHi over the pre-treatment control was 7.588 (standard deviation of 0.141) while in fish 7 pH_i was 7.594 (standard deviation of 0.138). The measured pH_i was comparable between fish and only varied in the second decimal place. They were slightly higher than the pH_i measured by Schmidt (2019), also in the head of polar cod. Schmidt (2019) measured pH_i in Polar cod in cranial tissues of about 7.50 (±0.5) under control conditions. The obtained pHi from ^{31}P-NMR spectroscopy appeared to be reliable. The acquisition time in aforesaid study (Schmidt 2019) was 18 minutes. The attained acquisition time of about 5 minutes per scan in this study was therefore substantially faster, allowing higher temporal resolution, while providing data of comparable quality.

The experimental protocol consisted of a post-handling acclimation phase, a pre-treatment control, the treatment period and a post treatment control. The post-handling acclimation phase was 18 hours, a pre-treatment control had a duration of 3 hours, the treatment was administered 24 hours and a post treatment control again had a duration of 3 hours.

Phase contrast imaging showed blood flow in vessels ranging from 0.15 cm/s and 0.71 cm/s in vessels of different diameter in the head of polar cod. Measured flow velocity was comparable between animals. Schmidt (2019) measured blood flow in arteries and veins of polar cod and measured flow velocities in the dorsal aorta of about 1.5 cm/s and flow velocities in the caudal vein of about 1.0 cm/s under control conditions.

The measured slow blood flows using FLASH showed comparable signal intensities between animals. Measurements within one animal stopped to be comparable when movement occurred, and signal intensities varied over time coinciding with movement.

As measurements were conducted in blocks consisting out of a tri-pilot scan, a FLASH scan, A BOLD scan, a phase contrast imaging scan and three ^{31}P-spectra each, the temporal resolution per method was limited. Only two scans per imaging method per hour could be obtained as well as two blocks of three consecutive spectra per hour. This circumstance could have led to a miss of very fast changes, both in blood

distribution and energy status. The temporal resolution might have been too low to properly investigate acute effects of elevate pCO_2 and immediate regulative responses. To eliminate this, uncertainty trials could be conducted where control and treatment conditions are induced and only one of the methods, either MR imaging or NMR-spectroscopy is used over the whole course of the experiment. Additionally, the application of only three hours of control prior and post the treatment appears short. If movement of the fish happened during the control phase a considerable number of scans can be lost for evaluation due to movement artefacts. Therefore, it appears advisable to extend the control phases in potential follow up studies.

6.2 Effects of Ocean Acidification

Over the course of this study an array of methods was adapted to the *in vivo* investigation of the blood distribution of polar cod and an experimental protocol was developed. The presented study attained to deliver the first multi-parametric datasets, investigating blood supply on different levels of the vascular system of the head combined with observations of the acid-base and energy status of the brain of polar cod.

As ^{31}P-NMR spectroscopy was conducted in 7 animals a big stability in pH_i under control conditions has been observed. Changes in pH_i were observed between pre-treatment control and treatment and between treatment and post-treatment control. The pH_i in brain cells of polar cod decreased when the treatment conditions were administered. This decrease was subtle and was compensated for within 24 hours.

The brain cells pH_i was affected but compensated for within 24 hours. Schmidt (2019) observed non-significant reductions in pH_i in Polar cod under ocean acidification in cranial tissues from ~7.50 under control conditions to ~7.45 under 1668 ± 250 µatm CO_2 at the first day of treatment and a recovery at day 2. In this study, under treatment conditions a mean pH_i of 7.531 (standard deviation of 0.116) was measured for fish 6 and for fish 7 under treatment conditions was 7.585 (standard deviation of 0.133). even though, in this study, the treatment was far higher than in the study of Schmidt (2019)

the decrease in pH_i under treatment were substantially smaller. Like in Schmidts study, the pH_i regulation was complete within 24 hours. The energy status of the brain cells showed fluctuations, but no OA dependent pattern was identified. This might be due to the fact, that exhibited pH_i alterations where minor and did not need energy intensive regulation.

Under normal conditions pH is tightly controlled in organisms due to its critical role for the function of cellular processes such as the energy metabolism. While the measurement of blood pH (i.e. extracellular pH (pH_e)) is relatively simple, the accurate measurement of intracellular pH (pH_i) *in vivo* is more challenging. As gills are highly permeable to CO_2, acidosis induced by elevated environmental CO_2 can be experienced both extra- and intracellularly. There is lack of knowledge still to be filled about the extent of compensation mechanisms, the mechanisms and their phylogenetic distribution (Baker *et al.* 2009). Complete or substantial pH compensation was demonstrated in many species of fresh water and marine fish. Some species seem to be able to completely regulate pH_i (preferential pH_i regulation) of certain tissues like brain muscle and liver tissue albeit experiencing severe reduction in pH_e. In White sturgeon (*Acipenser transmontanus*) for example there appears to be a complete pH_i protection keeping pH_i stable under both transient and prolonged blood acidosis (Baker *et al*. 2009). Acid-base compensation might be affected by the water composition and is more displayed in marine species. In both, freshwater and marine fish (Cameron & Kormanik 1982) acid-base loads infused into the animals' blood will enter the intracellular compartment rapidly, but the change in pH_i is remarkably lower than in pH_e. This is due to the much greater buffer capacity of the intracellular compartment. At 6h after the infusion no significant differences in pH_i could be detected while the blood parameters recovered at the end of a 24h trial period (Cameron & Kormanik 1982).

The alterations in pH_i due to handling associated stress were notably stronger over the first hours post handling (Figure 5-24) than during treatment. This also suggests that the effect of OA on pH_i in the brain of polar cod might be of no big ecological significance.

The energetic status of the brain cells showed fluctuations over time. There was no obvious pattern detected nor a dependency of fluctuations to the treatment. In fish 6

both P_i-PCr-ratio and βATP were lower under treatment than under pre-treatment control. For fish 7, the opposite was the case and both indices were higher under treatment than under pre-treatment control. This can be explained considering that there might be no OA-dependent effect. Comparing these slight fluctuations to the alterations in the energetic status right after handling of the fish the effect appears negligible.

The peak of βATP was not clearly identifiable in all measurements due to the relatively low peak intensity and the low signal to noise ratio of the *in vivo* measurements. Therefore, the P_i-PCr-ratio appeared to be the better choice in this study.

To investigate potential changes in blood vessels of the head phase contrast imaging was used. In fish 6 changes in blood flow could be observed in two blood vessels comparing control and treatment conditions. The mean blood flow per scan seemed to be relatively stable over the whole trial showing small fluctuations that did not obviously coincide with the treatment and did not vary simultaneously. It is therefore not likely that the observed effect is correlated to the treatment. In fish 7 increases in measured blood flow were noted in one blood vessel. As this increase coincides with movement of the fish and the position of the ROI had to be adapted it cannot be concluded that this change is due to the treatment. In other observed blood vessel no trend or effects of the treatment could be identified.

The phase contrast imaging (FLOWMAP) scanning sequence used was based on a Bruker scanning protocol that is designed for „quantitative mapping of blood velocity in heart and large vessels" (Operating Manual PV6.01.). The selectable flow velocity in the examination parameters where higher than the flow velocities expected in polar cod. This may partially be responsible for the relatively high standard deviations. The selection of different phase contrast imaging protocol might allow more accurate measurements. The extent of the accuracy of the flow velocity determination in this study did not seem to be a limiting factor as measurements were comparable amongst vessels, animals and to literature (Schmidt 2019).

In this study the evaluation of phase contrast images was conducted using two different approaches. First, the evaluation of one single polygon-shaped ROI covering the whole cross-section of the brain and second the evaluation of various smaller rectangular

ROIs. When comparing the bigger polygon ROIs that cover the whole cross-section of the brain to the smaller rectangular ROIs covering only parts of it, differences could be noted. Loss of track of vessel happened occasionally due to movement of the fish. This circumstance, of course limited the comparability of measurements. This method was especially susceptible for this issue as the ROIs were so small and only covering individual blood vessels. Even slight movements were problematic as small adjustments of the angle of the fish to the imaging plane could alter the diameter of the blood vessel at the position of the scan. The advantage, and what makes it unique in the set of tested techniques, of the phase contrast imaging is that it allows to quantify blood flow.

In fish 6 in two ROIs an increase in signal intensity was observed and a decrease in signal intensity in one ROI. The one ROI showing a decrease in signal intensity was the one covering the whole cross section of the brain while the two ROIs showing an increase where two small ROIs positioned within the big one. This variation cannot be explained easily and further investigations of fluctuations local variations in blood flow in the brain on a smaller scale are needed.

As changes in blood flow observed in fish 7 coincide with movement of the fish they must be considered with care. In ROI 2 coinciding with movement a drastic decrease in signal intensity was notable. In ROI 3 again an increase could be observed. The data in ROI 4 gives no clear trend. Beside this episode of alterations in signal intensity when movement happened there were no strong alterations or fluctuations noted. In both fish no effect of the treatment on the blood flow could be identified.

The FLASH imaging was expected to be less affected by movements as the ROIs were fewer and bigger and therefore loss of track was not considered as much of an issue. Also, the fewer number of ROIs allowed easier readjustment in the case of a movement and a loss of the underlying feature was very unlikely. This was only partially true as movements in fish 7 probably caused the strong alterations in signal intensity. Other than phase contrast imaging FLASH only allows to detect relative changes but not to quantify blood flow.

The BOLD imaging in fish 6 was affected by movement of the fish to a degree that no pre-treatment control could be obtained. Detected signal intensities in the ROI 1 did

vary slightly but no trend was observable. In ROI 2 a strong increase in signal intensity was measured till circa 2 h after treatment began. After this peak, a decline seemed to start. In ROI 3 the contrary could be observed as the values decreased. This observation has no obvious interpretation but might be caused by differing activity in certain areas of the brain. In fish 7, the position of the ROIs had to be rearranged 6 times and 17 scans could not be evaluated due to movement artefacts. Movement was limiting the analysis. After 1 hour of treatment there appeared to be an increase in signal intensity in ROI 1 and 2 and an slight decrease in ROI 3. After 4 hours there was another increase in signal intensity in ROI 1 and 2 leading to a peak at 9 hours after the begin of treatment and then reducing again. These observed fluctuations in oxygenated haemoglobin do not obviously coincide with the treatment but a correlation cannot be excluded.

Very similar to the FLASH imaging, BOLD imaging was expected to be less affected by movements as the ROIs were fewer and bigger than in phase contrast imaging. Also, the fewer number of ROIs allowed easier readjustment in the case of a movement and a loss of the underlying feature was very unlikely. Other than phase contrast imaging BOLD only allows to detect relative changes but not to quantify blood flow, resp. perfusion.

Even though, fluctuations in blood distribution in blood vessels and blood oxygenation could be observed, no clear pattern was observed and no OA dependent effect on these processes was identified.

In air breathing animals cerebral blood flow (CBF) increases under hypercapnia (Siesjö 1978). Ocean acidification due to increased pCO_2 induces hypercapnia in fish (Ishimatsu *et al.* 2005) and many behavioural alterations have been described in fish under ocean acidification, e.g. altered reaction to olfactory cues (see Tresguerres & Hamilton 2017 for a review). This study could not find increased CBF under OA. The only study that investigated CBF under hypercapnia, known by the author, found increased blood flow in the optic lobe of rainbow trout (*Oncorhynchos mykiss*) and unchanged blood flow in the optic lobe of crucian carp (*Carassius carassius*) (Söderström & Nilsson 2000). These results point out that there might be strong species differences.

Other than in air-breathing animals, in water-breathing teleost fish, ventilation control is driven not only by CO_2/pH-dependent mechanisms but also and more importantly by O_2-dependent mechanisms (Gilmour 2000). Very little is known about the regulating mechanism of CBF in lower vertebrates like fish. In air breathing vertebrates like mammals, hypercapnia induces increases in CBV due to mechanisms that include nitric oxide production. The mechanism in teleost fish remain unclear but appear to be independent of nitric oxide production (Söderstrom & Nilsson 2000). Söderstrom & Nilsson (2000) suggest that increases in CBF might occur in fish species that also exhibit increased ventilation rates under hypercapnia. Wermter *et al*. (2018) discuss movement artefacts potentially due to increased ventilation in polar cod under hypercapnia. Many teleost species exhibit hyperventilation under hypercapnia (Ishimatsu et al. 2005) but some species, e.g. the goldfish (*Carassius auratus*) show no such response (Söderstrom & Nilsson 2000). Schmidt (2019) showed increases in ventilation rate in polar cod under hypercapnia (1668 ± 250 µatm CO_2).

7 Conclusion

This thesis aimed to adapt a set of techniques to investigate the potential effects of OA on the blood distribution, pH_i and energy status of brain cells in polar cod. A suitable array of techniques was adapted. MR imaging techniques such as phase contrast imaging, FLASH imaging and BOLD imaging were used to investigate potential changes in blood distribution both in blood vessels and perfusion. No effect of ocean acidification on the blood distribution could be identified. Neither in phase contrast imaging, nor slow blood flow or BOLD were changes observed that obviously coincided with the treatment administering. Small decreases in pH_i occurred when OA was induced. But these changes were compensated completely within 24 hours. No obvious patterns in the energetic status of the brain cell were documented as reaction to induced OA. As changes in the blood distribution and cerebral blood flow were not observed under high CO_2 concentrations, they are unlikely to be underlying cause of the behavioural alterations observed under OA.

For successor studies, temporal resolution should be increased, and control periods extended. Future studies on potential changes in blood distribution under hypercapnia in teleost fish should consider assessing ventilation changes as supporting measure. Future work could refine the perfusion-weighted imaging approaches and use BOLD-imaging to assess potential small-scale regional differences in the perfusion of brain to investigate for example whether regions associated with affected functions are perfused differently under hypercapnia. For example, there are studies suggesting altered olfaction in fish like under OA, therefor it might be interesting to investigate potential perfusion changes in the olfactory bulb.

Considering that polar cod is a key species of the arctic food web, threatened by climate change the investigation of the causes of observed behavioural alteration under OA seems highly likely. Although this study did not find a cause it advanced the knowledge about blood distribution in polar cod and helped to discard potential underlying but now unlikely factors. Besides this, this study broadened the knowledge about the vascularisation in the head of polar cod advanced the application of *in vivo* MRI in marine animals.

8 Acknowledgements

My personal thanks belong to Dr. Christian Bock, first for accepting me as his thesis student and offering me this amazing opportunity and second for his tireless support. Bastian Maus M.Sc., I have to thank for answering all my thousands of questions, for his help troubleshooting and overcoming many problems and enlighten me so often.

Many thanks to Clara Scheuring, B.Sc. for the amazing collaboration and the many hours in the NMR lab that would have been far less funny without her. Thanks to Svenja Neumann B.Sc. for her help and corrections.

Thank´s to Sabrina Hüpperling B.Sc, for her unparalleled support and matchless backing.

Thanks to my parents who supported me always and unconditional.

I am very grateful for the opportunity to conduct my thesis research at the NMR lab at the AWI in Bremerhaven. A warm thanks belongs to all the members of the section IEP who supported me on this journey. Furthermore, I like to thank Hans-Otto Pörtner for giving me the opportunity to work in his section on this interesting topic.

Also, many thanks belong to the IMBRSea coordination and all the wonderful people that allow this incomparable programme to exist.

Furthermore, I must thank Mrs. Klingele for her relentless support and encouragement that helped shaping my way.

9 References

Alexander, M. A.; Scott, J. D.; Friedland, K. D.; Mills, K. E.; Nye, J. A.; Pershing, A. J.; Thomas, A. C. (2018): Projected sea surface temperatures over the 21st century: Changes in the mean, variability and extremes for large marine ecosystem regions of Northern Oceans. In: Elem Sci Anth 6 (1), S. 9. DOI: 10.1525/elementa.191.

Baker, D. W.; Matey, V.; Huynh, K. T.; Wilson, J. M.; Morgan, J. D.; Brauner, C. J. (2009): Complete intracellular pH protection during extracellular pH depression is associated with hypercarbia tolerance in white sturgeon, Acipenser transmontanus. In: American journal of physiology. Regulatory, integrative and comparative physiology 296 (6), R1868-80. DOI: 10.1152/ajpregu.90767.2008.

Beirnaert, C., Meysman, P., Vu, T. N., Hermans, N., Apers, S., Pieters, L., … Laukens, K. (2018). speaq 2.0: A complete workflow for high-throughput 1D NMR spectra processing and quantification. PLOS Computational Biology, 14(3), e1006018. doi:10.1371/journal.pcbi.1006018

Bickler, P. E. (1992). Effects of temperature and anoxia on regional cerebral blood flow in turtles. American Journal of Physiology-Regulatory, Integrative and Comparative Physiology, 262(3), R538–R541. doi:10.1152/ajpregu.1992.262.3.r538

Bock, C.; Sartoris, F.; Wittig, R-M.; Pörtner, H.-O. (2001): Temperature-dependent pH regulation in stenothermal Antarctic and eurythermal temperate eelpout (Zoarcidae): an in-vivo NMR study. In: Polar Biology 24 (11), S. 869–874. DOI: 10.1007/s003000100298.

Borger, R., De Boeck, G., Van Audekerke, J., Dommisse, R., Blust, R., Van der Linden, A. (1998): Recovery of the Energy metabolism after Hypoxic Challenge at Different temperature Conditions. A 31P-NMR Spetroscopy Study With Common Carp. In: Comparative Biochemistry and Physiology Part A (130).

Bruker BioSpin MRI GmbH: OPERATING MANUAL_PV6.0.1.

Buchanan, J. E., & Phillis, J. W. (1993). The role of nitric oxide in the regulation of cerebral blood flow. Brain Research, 610(2), 248–255. doi:10.1016/0006-8993(93)91408-k

References

Cameron, J. N.; Kormanik, G. A. (1982): Intracellular and extracellular acid-base status as a function of temperature in the freshwater channel catfish, Ictalurus punctatus In: Journal of Experimental Biology 99: 127-142;

Claiborne, J. B.; Edwards, S. L.; Morrison-Shetlar, A. I. (2002): Acid-base regulation in fishes: cellular and molecular mechanisms. In: The Journal of experimental zoology 293 (3), S. 302–319. DOI: 10.1002/jez.10125.

Dahlke, F. T., Butzin, M., Nahrgang, J., Puvanendran, V., Mortensen, A., Pörtner,H.-O., Storch, D. (2018): Northern cod Species Face Spawning Habitat Losses if Global Warming Exceeds 1.5°C. In: Science Advances (4).

Drost, H. E.; Carmack, E. C.; Farrell, A. P. (2014): Upper thermal limits of cardiac function for Arctic cod Boreogadus saida, a key food web fish species in the Arctic Ocean. In: Journal of fish biology 84 (6), S. 1781–1792. DOI: 10.1111/jfb.12397.

Duelli, R.; Kuschinsky, W. (1993): Changes in Brain Capillary Diameter during Hypocapnia and Hypercapnia. In: Journal of Cerebral Blood Flow and Metabolism (13), S. 1025–1028.

Esbaugh, A. J. (2018): Physiological implications of ocean acidification for marine fish: emerging patterns and new insights. In: Journal of comparative physiology. B, Biochemical, systemic, and environmental physiology 188 (1), S. 1–13. DOI: 10.1007/s00360-017-1105-6.

Field, C. B.; Barros, V. R., Dokken, D. J.; Mach, K.J.; Mastrandrea, M.D.; Bilir, T.E.; Chatterjee, M. ; Ebi, K.L.; Estrada, Y.O.; Genova, R.C.; Girma, B. ; Kissel, E.S.; Levy, A.N.; MacCracken, S.; Mastrandrea, P.R.; and White, L.L. (eds.) Climate Change 2014: Impacts, Adaptation, and Vulnerability. Part A: Global and Sectorial Aspects. Working Group II Contribution to the Fifth Assessment Report of the Intergovernmental Panel on Climate Change. New York, NY: Cambridge University Press; 2014.

Fransson, A.; Chierici, M.; Nojiri, Y. (2009): New insights into the spatial variability of the surface water carbon dioxide in varying sea ice conditions in the Arctic Ocean. In: Continental Shelf Research 29 (10), S. 1317–1328. DOI: 10.1016/j.csr.2009.03.008.

References

Gaston, A. J.; Woo, K.; and Hipfner, J. M. (2003): Trends in Forage Fish Populations in Northern Hudson Bay since 1981, as Determined from the Diet of Nestling Thick-Billed Murres Uria lomvia. In: Arrctic, S. 227–233.

Gattuso, J-P; Magnan, A.; Billé, R.; Cheung, W. W. L.; Howes, E. L.; Joos, F. et al. (2015): OCEANOGRAPHY. Contrasting futures for ocean and society from different anthropogenic CO_2 emissions scenarios. In: Science (New York, N.Y.) 349 (6243), aac4722. DOI: 10.1126/science.aac4722.

Gesser, H., & Poupa, O. (1983). Acidosis and cardiac muscle contractility: Comparative aspects. Comparative Biochemistry and Physiology Part A: Physiology, 76(3), 559–566. doi:10.1016/0300-9629(83)90458-9

Gesser, H.; Jorgensen, E. (1982): pHi, contractility and Ca-balance under hypercapnic acidosis in the myocardium of different vertebrate species. In: Journal of Experimental Biology 96: 405-412;

Gilmour, K. M. (2001): The CO2/pH Ventilatory Drive in Fish. In: Comparative Biochemistry and Physiology Part A (130), S. 219–240.

IPCC (2018): Summary to Policymakers of IPCC Special report on Global Warming od 1.5°C Approved by Governments.

Ishimatsu, Atsushi (2005): Physiological effects on fishes in a high-CO 2 world. In: J. Geophys. Res. 110 (C9), S. 333. DOI: 10.1029/2004JC002564.

Matthaei, D., Frahm, J., Haase, A., & Hanicke, W. (1985). Regional Physiological Functions Depicted by Sequences of Rapid Magnetic resonance. In: The Lancet, *326(8460), 893.* doi:10.1016/s0140-6736(85)90158-8

McKendry, J. E. and Perry, S. F. (2001): Cardiovascular effects of hypercarbia in trout. In: The Journal of experimental biology, S. 115–125.

Jutfelt, F.; and Hedgärde, M. (2013): Atlantic cod actively avoid CO2 and predator odour, even after long-term CO2 exposure. In: Frontiers in zoology (10).

Kost, G. J. (1990): pH standardization for phosphorus-31 magnetic resonance heart spectroscopy at different temperatures. In: Magnetic resonance in medicine (14).

References

Kunz, K. L.; Claireaux, G.; Pörtner, H.-O.; Knust, R.; Mark, F. C. (2018): Aerobic capacities and swimming performance of polar cod (Boreogadus saida) under ocean acidification and warming conditions. In: The Journal of experimental biology 221 (Pt 21). DOI: 10.1242/jeb.184473.

Mark, F. C. (2018): Links to master tracks in different resolutions of HEINCKE cruise HE519, Trondheim - Bremerhaven, 2018-09-21 - 2018-10-16. *Alfred Wegener Institute, Helmholtz Centre for Polar and Marine Research, Bremerhaven*, PANGAEA, https://doi.org/10.1594/PANGAEA.896258

Mueter, Franz J.; Nahrgang, Jasmine; John Nelson, R.; Berge, Jørgen (2016): The ecology of gadid fishes in the circumpolar Arctic with a special emphasis on the polar cod (Boreogadus saida). In: Polar Biol 39 (6), S. 961–967. DOI: 10.1007/s00300-016-1965-3.

Ogawa, S., Lee, T.M., Kay, A. R., Tanke, D.W. (1990): Brain Magnetic Resonance Imaging With Contrast Dependent on Blood Oxygenation. In: Proceedings of the National Academy of Sciences (87), S. 9868–9872.

Perry, S. F.; Gilmour, K. M. (2006): Acid-base balance and CO2 excretion in fish: unanswered questions and emerging models. In: Respiratory physiology & neurobiology 154 (1-2), S. 199–215. DOI: 10.1016/j.resp.2006.04.010.

Pierrot, D. E. Lewis,and D. W. R. Wallace. 2006. MS Excel Program Developed for CO2 System Calculations. ORNL/CDIAC-105a. Carbon Dioxide Information Analysis Center, Oak Ridge National Laboratory, U.S. Department of Energy, Oak Ridge, Tennessee. doi: 10.3334/CDIAC/otg.CO2SYS_XLS_CDIAC105a

Polyakov, Igor V.; Beszczynska, Agnieszka; Carmack, Eddy C.; Dmitrenko, Igor A.; Fahrbach, Eberhard; Frolov, Ivan E. et al. (2005): One more step toward a warmer Arctic. In: Geophys. Res. Lett. 32 (17), S. 1061. DOI: 10.1029/2005GL023740.

Pörtner, H. O., & Knust, R. (2007). *Climate Change Affects Marine Fishes Through the Oxygen Limitation of Thermal Tolerance. Science, 315(5808), 95–97.* doi:10.1126/science.1135471

References

Pörtner, H. (2008): Ecosystem effects of ocean acidification in times of ocean warming: a physiologist's view. In: Mar. Ecol. Prog. Ser. 373, S. 203–217. DOI: 10.3354/meps07768.

Riebesell, U., Fabry, V. J., Hansson, L., and Gattuso, J.-P.: Guide to best Practices for Ocean Acidification research and Data Reporting.

Roberts, J. K.M., Wade-Jardetzky, N., and Jardetzky O. (1981): Intracellular pH Measurements by 31P NMR. Influence of Factors Other Than pH on 31P Chemical Shifts. In: Biochemistry (20), S. 5389–5394.

Schmidt, M.; Gerlach, G.; Leo, E.; Kunz, K. L.; Swoboda, S.; Pörtner, H. O. et al. (2017): Impact of ocean warming and acidification on the behaviour of two co-occurring gadid species, Boreogadus saida and Gadus morhua, from Svalbard. In: Mar. Ecol. Prog. Ser. 571, S. 183–191. DOI: 10.3354/meps12130.

Schmidt, M.; Windisch, H. S.; Ludwichowski, K.-U.; Seegert, S. L. L.; Pörtner, H.-O.; Storch, D.; Bock, C. (2017): Differences in neurochemical profiles of two gadid species under ocean warming and acidification. In: Frontiers in zoology 14, S. 49. DOI: 10.1186/s12983-017-0238-5.

Schmidt, M. (2019): Behavioural disturbances and underlying neurophysiological mechanisms during ocean acidification and warming in Gadus morhua and Boreogadus saida. Dissertation zur Erlangung des akademischen Grades -Dr. rer. nat.

Siesjö, B. K.: Brain Energy Metabolism (1978): John Wiley and sons, New York.

Söderström, V.; Nilsson, G. E. (2000): Brain Blood Flow During Hypercapnia in Fish: No Role of Nitric Oxide. In: Brain Research (857), S. 207–211.

Soldatov, A. A. (2006): Organ blood flow and vessels of microcirculatory bed in fish. In: J Evol Biochem Phys 42 (3), S. 243–252. DOI: 10.1134/S002209300603001X.

Tresguerres, M.; Hamilton, T. J. (2017): Acid-base physiology, neurobiology and behaviour in relation to CO2-induced ocean acidification. In: The Journal of experimental biology 220 (Pt 12), S. 2136–2148. DOI: 10.1242/jeb.144113.

References

Underwood, S.R.; Firmin, D. N.; Klipstein, R. H., Rees, R. S.; Longmore, D. B; (1987): Magnetic Resonance Velocity Mapping: Clinical Application of a new Technique in British Heart Journal. 57;404-412

van den Thillart, G.; van Waarde, A.; Muller, H. J.; Erkelens, C.; Addink, A.; Lugtenburg, J. (1989): Fish muscle energy metabolism measured by in vivo 31P-NMR during anoxia and recovery. In: The American journal of physiology 256 (4 Pt 2), R922-9. DOI: 10.1152/ajpregu.1989.256.4.R922.

Wermter, F. C.; Maus, B.; Pörtner, H.-O.; Dreher, W.; Bock, C. (2018): CO2 induced pHi changes in the brain of polar fish: a TauCEST application. In: NMR in biomedicine 31 (8), e3955. DOI: 10.1002/nbm.3955.

Wickham, H. (2016): ggplot2: Elegant Graphics for Data Analysis. Springer-Verlag New York

10 Annex

The original data, 31P-NMR spectra, MR images and analysed blood flow velocities can be found in the digital annex. Movie files of the 3D rendered angiography scans can be found in the digital annex as well.

10.1 Phantom trials

Table 2 measured chemical shifts of the ^{31}P-NMR spectroscopy phantom trials.
All chemical shift for Pi, γATP, αATP and βATP in relation to PCr are in parts per million [ppm]. The column type revers to the phantom, pH was the set pH of the phantom, T refers to the temnperature of the trial, Lid to wether or not the chamber was sealed with a lid and flow if the medium was flowing at the time of the trial.

date	type	pH	Pi [ppm]	γATP [ppm]	αATP [ppm]	βATP [ppm]	lid	T	coil	medium	flow
20190218	p	6.8	4.7	3.71	7.86	18.57	N	room	3cm	air	NA
20190218	p	6.8	4.64	3.71	7.86	18.75	N	room	3cm	air	NA
20190218	p	6.8	4.64	3.84	7.92	18.75	N	room	3cm	air	NA
20190218	p	6.8	4.77	3.78	7.92	18.69	N	room	3cm	air	NA
20190218	p	6.8	4.7	3.78	7.92	18.75	N	room	3cm	air	NA
20190218	p	6.8	4.77	3.78	7.8	18.69	Y	room	3cm	air	NA
20190218	p	6.8	4.83	3.71	7.8	18.69	Y	room	3cm	air	NA
20190218	p	6.8	4.64	3.71	7.92	18.63	Y	room	3cm	air	NA
20190218	p	6.8	4.7	3.84	7.98	18.75	Y	room	3cm	air	NA
20190218	p	6.8	4.64	3.78	7.92	18.63	Y	room	3cm	air	NA
20190219	p	6.8	4.7	3.78	7.86	18.69	Y	room	3cm	air	NA
20190219	p	6.8	4.77	3.78	7.92	18.75	Y	room	3cm	air	NA
20190219	p	6.8	4.64	3.78	7.98	18.75	Y	room	3cm	air	NA
20190219	p	6.8	4.64	3.71	7.86	18.75	Y	room	3cm	air	NA
20190219	p	6.8	4.64	3.78	7.98	18.88	Y	room	3cm	air	NA
20190219	p	7	4.89	3.53	7.86	18.63	Y	room	3cm	air	NA
20190219	p	7	4.95	3.47	7.86	18.57	Y	room	3cm	air	NA
20190219	p	7	4.83	3.53	7.86	18.57	Y	room	3cm	air	NA
20190219	p	7	4.83	3.47	7.98	18.57	Y	room	3cm	air	NA
20190219	p	7	4.83	3.59	7.92	18.63	Y	room	3cm	air	NA
20190219	p	7.19	5.14	3.22	7.74	18.38	Y	room	3cm	air	NA
20190219	p	7.19	5.08	3.34	7.98	18.57	Y	room	3cm	air	NA
20190219	p	7.19	5.14	3.28	7.74	18.38	Y	room	3cm	air	NA
20190219	p	7.19	5.08	3.22	7.86	18.51	Y	room	3cm	air	NA
20190219	p	7.19	5.08	3.22	7.86	18.44	Y	room	3cm	air	NA
20190219	p	7.59	5.45	2.91	7.86	18.38	Y	room	3cm	air	NA
20190219	p	7.59	5.45	3.03	7.86	18.32	Y	room	3cm	air	NA
20190219	p	7.59	5.45	2.97	7.8	18.38	Y	room	3cm	air	NA
20190219	p	7.59	5.38	2.97	7.8	18.38	Y	room	3cm	air	NA
20190219	p	7.59	5.45	2.91	7.8	18.38	Y	room	3cm	air	NA
20190219	p	7.75	5.45	2.85	7.8	18.38	Y	room	3cm	air	NA
20190219	p	7.75	5.57	2.72	7.74	18.26	Y	room	3cm	air	NA

20190219	p	7.75	5.51	2.79	7.8	18.32	Y	room	3cm	air	NA
20190219	p	7.75	5.51	2.85	7.74	18.32	Y	room	3cm	air	NA
20190219	p	7.75	5.57	2.79	7.74	18.26	Y	room	3cm	air	NA
20190219	p	7.98	5.54	2.79	7.83	18.44	Y	room	3cm	air	NA
20190219	p	7.98	5.57	2.82	7.86	18.35	Y	room	3cm	air	NA
20190219	p	7.98	5.55	2.77	7.86	18.38	Y	room	3cm	air	NA
20190219	p	7.98	5.54	2.82	7.86	18.83	Y	room	3cm	air	NA
20190219	p	7.98	5.54	2.82	7.86	18.44	Y	room	3cm	air	NA
20190221	p	7.98	5.63	2.79	7.8	18.32	Y	room	3cm	air	NA
20190221	p	7.98	5.51	2.85	7.86	18.44	Y	room	3cm	air	NA
20190221	p	7.98	5.51	2.79	7.8	18.38	Y	room	3cm	air	NA
20190221	p	7.98	5.57	2.79	7.86	18.38	Y	room	3cm	air	NA
20190221	p	7.98	5.63	2.79	7.8	18.38	Y	room	3cm	air	NA
20190221	p	7.98	5.57	2.85	7.8	18.38	Y	room	2cm	air	NA
20190221	p	7.98	5.57	2.72	7.8	18.32	Y	room	2cm	air	NA
20190221	p	7.98	5.51	2.85	7.8	18.26	Y	room	2cm	air	NA
20190221	p	7.98	5.57	2.72	7.8	18.32	Y	room	2cm	air	NA
20190221	p	7.98	5.51	2.79	7.8	18.38	Y	room	2cm	air	NA
20190221	p	7.98	5.57	2.72	7.8	18.38	N	room	2cm	air	NA
20190221	p	7.98	5.51	2.79	7.86	18.44	N	room	2cm	air	NA
20190221	p	7.98	5.51	2.79	7.8	18.38	N	room	2cm	air	NA
20190221	p	7.98	5.57	2.72	7.8	18.32	N	room	2cm	air	NA
20190221	p	7.98	5.51	2.72	7.86	18.32	N	room	2cm	air	NA
20190221	p	7.98	5.51	2.79	7.8	18.38	Y	room	2cm	sw	n
20190221	p	7.98	5.51	2.72	7.74	18.32	Y	room	2cm	sw	n
20190221	p	7.98	5.51	2.79	7.8	18.32	Y	room	2cm	sw	n
20190221	p	7.98	5.57	2.79	7.8	18.32	Y	room	2cm	sw	n
20190221	p	7.98	5.51	2.72	7.8	18.32	Y	room	2cm	sw	n
20190221	p	7.98	NA	NA	NA	NA	Y	room	3cm	sw	n
20190221	p	7.98	NA	NA	NA	NA	Y	room	3cm	sw	n
20190221	p	7.98	NA	NA	NA	NA	Y	room	3cm	sw	n
20190221	p	7.98	NA	NA	NA	NA	Y	room	3cm	sw	n
20190221	p	7.98	NA	NA	NA	NA	Y	room	3cm	sw	n
20190222	p	7.98	5.51	2.78	7.74	18.36	Y	0	2cm	sw	y
20190222	p	7.98	5.51	2.82	7.77	18.36	Y	0	2cm	sw	y
20190222	p	7.98	5.55	2.73	7.81	18.45	Y	0	2cm	sw	y
20190222	p	7.98	5.51	2.82	7.91	18.45	Y	0	2cm	sw	y
20190222	p	7.98	5.51	2.73	7.72	18.4	Y	0	2cm	sw	y

10.1.1 Titration curve

Creation of a titration curve as reference for the *in vivo* ^{31}P-NMR Spectroscopy

As the pH-value of the second proton dissociation of the inorganic phosphate is close to neutrality the measured chemical shift of Pi can be transformed into a pH. As the

concentration of Pi are way higher within the cellular space than in the extracellular space this signal is mostly representing the intracellular milieu and is therefore transformable into an intracellular pH (pHi). As reference for the measured chemical shift reference measurements were performed using six phantoms with defined pH-values in the relevant pH-spectrum ranging from pH 6.8 up to 8. Each phantom was scanned five times with same MRI scanner and 31P-surface coil that were used in the *in vivo* experiments. The phantoms were glass spheres filled with a solution that aimed to simulate the "neurochemical cocktail" in the fish brain (see figure Figure 10-1 Photo of a phantom solution injected into a sealed glass vial. The vial was positioned within an experimental chamber.). It was based on a phosphate buffered saline (PBS) to which adenosine tri-phosphate (ATP), phosphocreatine (PCr), gamma-Aminobutyric acid (GABA), taurine (Tau), glutamine (Gln) and glutamic acid (Glu) were added in physiological concentrations. The desired pH-values were achieved by step-wise adding KOH. The exact concentrations can be found in Table 3.

Table 3 chemical composition of the ^{31}P-NMR Spectroscopy phantoms

substance	mass [g]	concentration [mM]
NaCl	1.924	137.2
KCl	0.045	2.5
Na_2HPO_4	0.117	1.8
KH_2PO_4	0.0572	1.8
PCr	0.425	8.4
ATP	0.61	5
GABA	0.05	2
Glutamine	0.072	2.1
Glutaminic acid	0.31	8.8
Taurine	0.063	2.1

Figure 10-1 Photo of a phantom solution injected into a sealed glass vial. The vial was positioned within an experimental chamber.

The respective solutions were stored in falcon tubes at 4°C to reduce hydrolysis of the ATP during storage. The samples were then transferred to sealed spherical glass vials for the NMR scans. The transfer was performed with a syringe to reduce air bubbles in the vial. The glass vial was mounted on and positioned with orthodontic wax within the in-house built animal chamber. First trials for positioning were performed without a lid closing the chamber and with the ^{31}P surface coil directly fixated onto the vial (see Figure 10-1). Directly after this measurement were completed the lid was added and the surface coil attached on top of the lid. After these measurements, obtained spectra were compared for possible differences in the apparent chemical shift and/or signal intensity, resp. signal-to-noise-ratio.

From the measurements at pH 6.8 to pH 8 a titration curve was plotted (see Figure 10-2).The exact measured values can be found in the annex (see Table 2). The model drm for dose response modelling from the R package drc was used (drm(data,, fct = LL.4()) (Christian Ritz and Jens C. Streibig, drc package for R))to generate titration curves fitted to the measured chemical shifts. The titration curves can be used to deviate the *in vivo* pH_i in by the measured chemical shifts. Titration curves were modelled for all phosphates contained in the samples. The fitted titration curves based on the measured chemical shifts of Pi, γATP, αATP and βATP in relation to PCr were not equally reliable, resp. well fitted. The curves for Pi and also γATP were well fitted. The curves for αATP and βATP were very bad fitted eventhough also based on the same dose-response-method (drm).

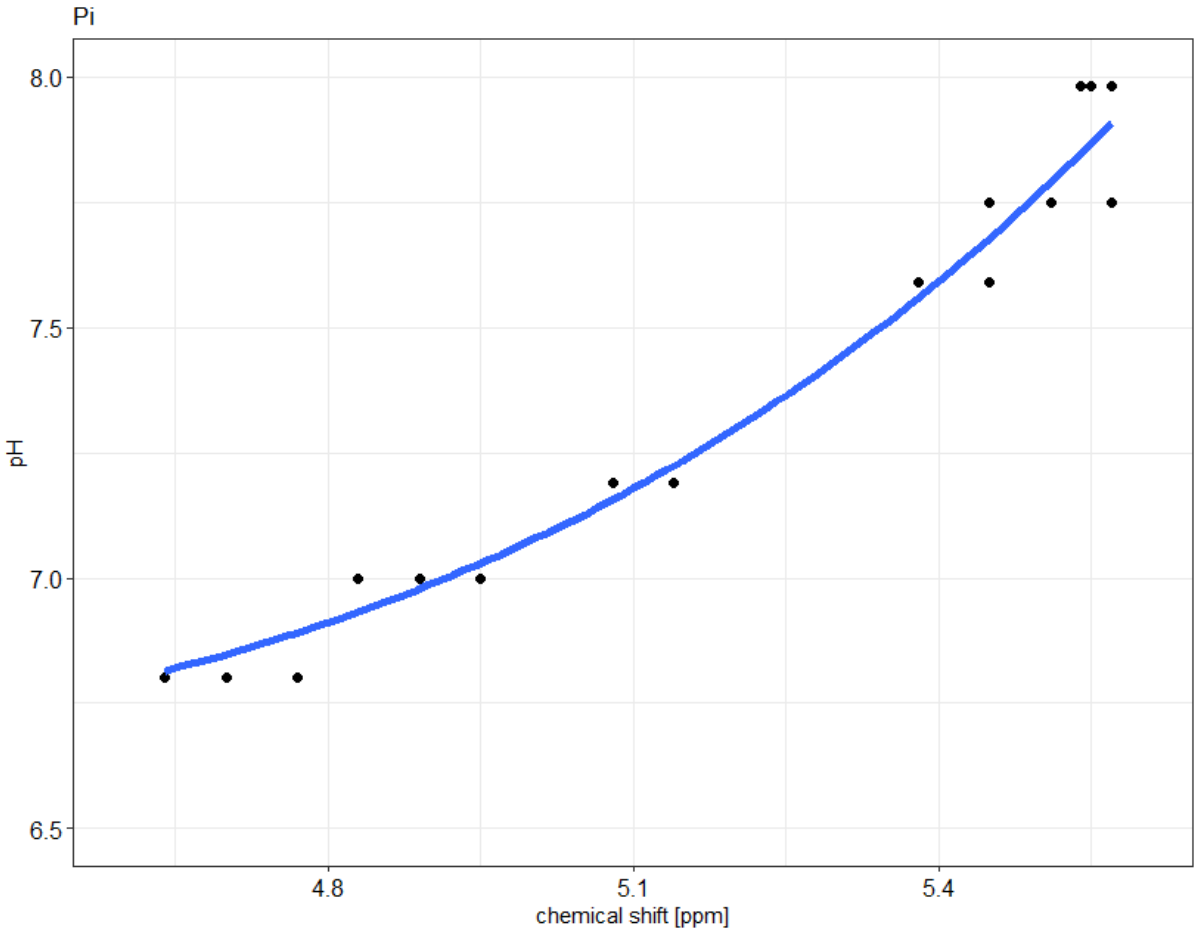

Figure 10-2 Titration curve.
Titration curve plotted from measurements of the chemical shift of Pi in relation to PCr at pH 7.98, 7.75, 7.59, 7.19, 7.00, 6.80. Each measurement was repeated five times. The blue curve indicates the drm model generated with the R packages drc with fct = LL.4())